AD-A092 900 DAVID W TAYLOR NAVAL SHIP RESEARCH AND DEVELOPMENT CE--ETC F/G 20/4
SIMULATION OF FULL-SCALE SHIP WAKE DISTRIBUTION BY A SEMI-GEOSI--ETC(U)
AUG 80 Y T SHEN, K D REMMERS, H T WANG

UNCLASSIFIED DTNSRDC/SPD-0944-01 NL

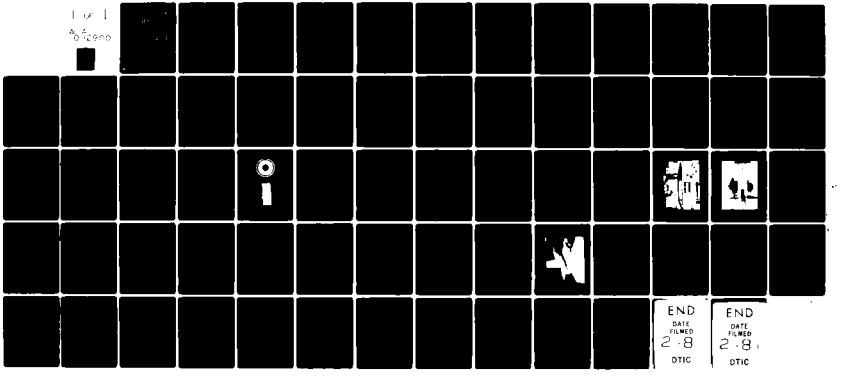

END DATE FILMED 2-81 DTIC

END DATE FILMED 2-81 DTIC

AD A092900

DTNSRDC/SPD-0944-01

DAVID W. TAYLOR NAVAL SHIP RESEARCH AND DEVELOPMENT CENTER

Bethesda, Maryland 20084

LEVEL II

(12)

SIMULATION OF FULL-SCALE SHIP WAKE DISTRIBUTION BY A SEMI-GEOSIM MODEL

by

Y.T. Shen, K.D. Remmers

and

H.T. Wang

DTIC
ELECTE
DEC 16 1980
S D
E

APPROVED FOR PUBLIC RELEASE: DISTRIBUTION UNLIMITED

* SHIP PERFORMANCE DEPARTMENT REPORT

80

August 1980

DTNSRDC/SPD-0944-01

SIMULATION OF FULL-SCALE SHIP WAKE DISTRIBUTION
BY A SEMI-GEOISM MODEL

DDC FILE COPY

NOW-DTNSRDC 5602/30 (2-80)
(supersedes 3960/46)

MAJOR DTNSRDC ORGANIZATIONAL COMPONENTS

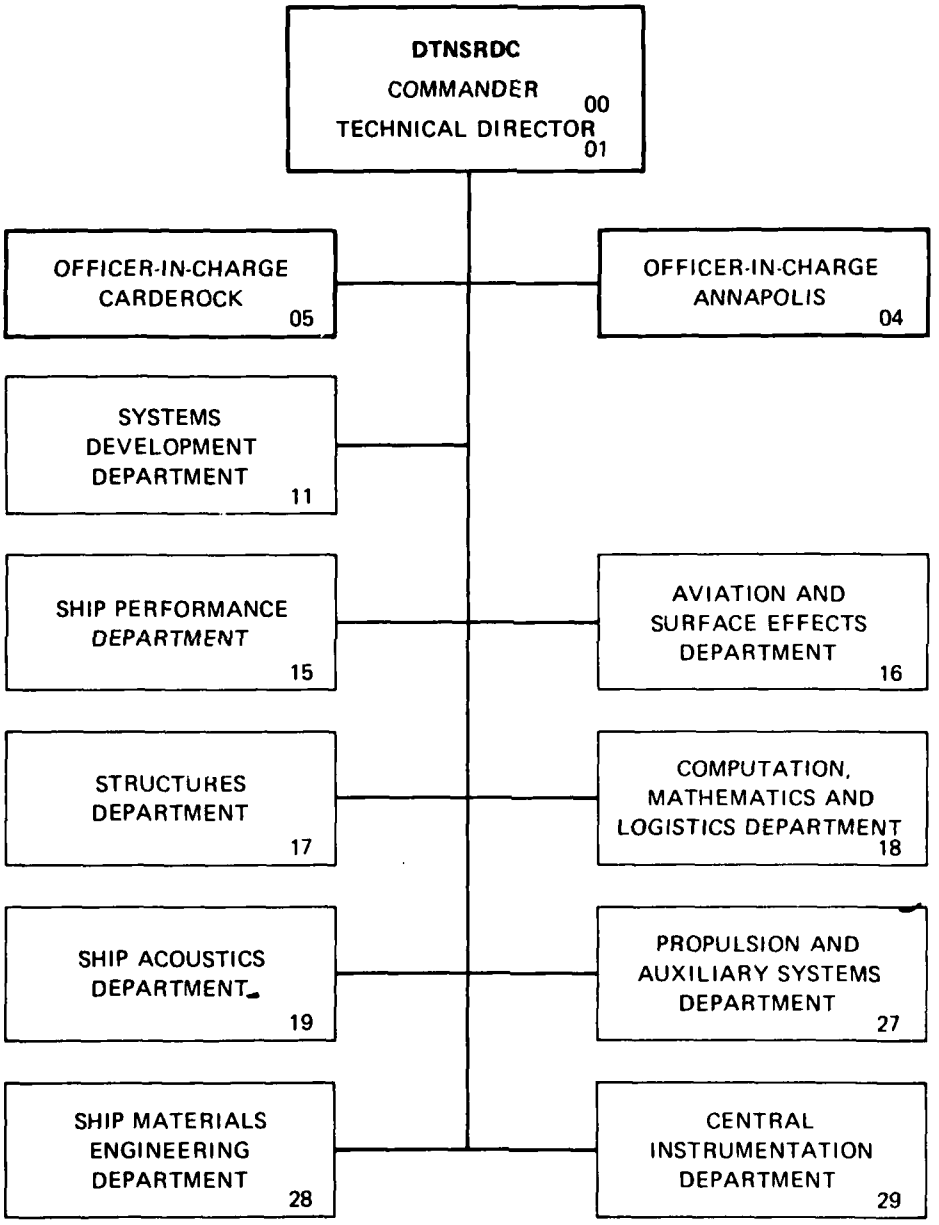

UNCLASSIFIED

SECURITY CLASSIFICATION OF THIS PAGE (When Data Entered)

REPORT DOCUMENTATION PAGE	READ INSTRUCTIONS BEFORE COMPLETING FORM
1. REPORT NUMBER: DTNSRDC/SPD-0944-01	2. GOVT ACCESSION NO.: AD-A092 900
3. RECIPIENT'S CATALOG NUMBER:	
4. TITLE (and Subtitle): Simulation of Full-Scale Ship Wake Distribution by a Semi-Geosim Model.	5. TYPE OF REPORT & PERIOD COVERED: Research and Development
	6. PERFORMING ORG. REPORT NUMBER:
7. AUTHOR(s): Y.T. Shen, K.D. Remmers and H.T. Wang	8. CONTRACT OR GRANT NUMBER(s):
9. PERFORMING ORGANIZATION NAME AND ADDRESS: David W. Taylor Naval Ship R&D Center, Navy Department, Bethesda, MD 20084	10. PROGRAM ELEMENT, PROJECT, TASK AREA & WORK UNIT NUMBERS: Work Unit Numbers: 1524-650 and 1524-703
11. CONTROLLING OFFICE NAME AND ADDRESS: David W. Taylor Naval Ship R&D Center, IRED Program, Bethesda, MD 20084	12. REPORT DATE: August 1980
	13. NUMBER OF PAGES: 65
14. MONITORING AGENCY NAME & ADDRESS (if different from Controlling Office)	15. SECURITY CLASS. (of this report): UNCLASSIFIED
	15a. DECLASSIFICATION/DOWNGRADING SCHEDULE:

16. DISTRIBUTION STATEMENT (of this Report)

APPROVED FOR PUBLIC RELEASE: DISTRIBUTION UNLIMITED

17. DISTRIBUTION STATEMENT (of the abstract entered in Block 20, if different from Report)

18. SUPPLEMENTARY NOTES

19. KEY WORDS (Continue on reverse side if necessary and identify by block number)

Semi-Geosim Model
Wake Simulation
Cavitation
Boundary Layer
Axisymmetric Body

20. ABSTRACT (Continue on reverse side if necessary and identify by block number)

Proper evaluation of the cavitation performance of a model propeller requires that as large a propeller as possible be tested so that the deviation in geometric similarity due to fabrication can be minimized. Propeller-tip cavitation inception is known to be Reynolds number dependent. Minimization of the scale effect also requires use of a large sized model propeller to achieve a high Reynolds number. Additionally, kinematic similarity requires that the radially varied inflow distribution at the

DD FORM 1 JAN 73 1473 EDITION OF 1 NOV 65 IS OBSOLETE S/N 0102-LF-014-6601

UNCLASSIFIED

SECURITY CLASSIFICATION OF THIS PAGE (When Data Entered)

UNCLASSIFIED

ABSTRACT (Continued)

propeller plane anticipated for a full-scale ship, must be properly simulated in the model tests. However, the geometric dimensions of the water tunnel present a constraint on the model size allowed. These conflicting demands have led to development of a semi-geosim ship model. The present report documents the measured, radially varied inflow distribution at the propeller plane of a semi-geosim model with various combinations of mesh screens on the body surface and lengths of the parallel middle body. Experimental results at the 36-inch(91cm) water tunnel indicate that the target wake of a representative axi-symmetric ship body may be reasonably simulated to the propeller tip by a semi-geosim model with a propeller 14 in. (35.6 cm) in diameter.

Accession For
NTIS GRA&I
DDC TAB
Unannounced
Justification
By
Distribution/
Availability Codes
Dist | Avail and/or special
A

TABLE OF CONTENTS

LIST OF FIGURES

LIST OF FIGURES (Continued)

LIST OF TABLES

NOMENCLATURE

C_A	Ship correlation allowance
C_F	Skin friction coefficient
C_P	Pressure coefficient
C_S	Surface area coefficient
C_V	Volume coefficient
D	Maximum body diameter of the axisymmetric body
D_P	Propeller diameter
r	Local radial distance from the centerline of the axisymmetric body
R_P	Propeller radius
u	Mean axial velocity around a circumferential plan
$\frac{\Delta u}{V}$	Velocity increment due to Reynolds number correction between model and full scale ship
w	Nominal wake fraction

ABSTRACT

Proper evaluation of the cavitation performance of a model propeller requires that as large a propeller as possible be tested so that the deviation in geometric similarity due to fabrication can be minimized. Propeller-tip cavitation inception is known to be Reynolds number dependent. Minimization of the scale effect also requires use of a large sized model propeller to achieve a high Reynolds number. Additionally, kinematic similarity requires that the radially varied inflow distribution at the propeller plane anticipated for a full-scale ship, must be properly simulated in the model tests. However, the geometric dimensions of the water tunnel present a constraint on the model size allowed. These conflicting demands have led to development of a semi-geosm ship model. The present report documents the measured, radially varied inflow distribution at the propeller plane of a semi-geosim model with various combinations of mesh screens on the body surface and lengths of the parallel middle body. Experimental results at the 36-inch (91 cm) water tunnel indicate that the target wake of a representative axisymmetric ship body may be reasonably simulated to the propeller tip by a semi-geosim model with a propeller 14 in. (35.6 cm) in diameter.

ADMINISTRATION INFORMATION

This work was performed under the In-House Independent Research and Exploratory Development Program of the David W. Taylor Naval Ship Research and Development Center (DTNSRDC) (Work Unit Numbers 1524-650 and 1524-703).

INTRODUCTION

When a propeller operates behind a ship hull, it operates in a non-uniform wake with a significant radially varying inflow. The most significant effect due to this wake distribution is to change the angle of attack on the propeller blades. Compared to operation in uniform inflows, wake operation causes dramatic increase of critical inception indices and strong amplitude modulation of cavitation noise spectra.[1,2*]

The previous approach taken at the David W. Taylor Naval Ship Research and Development Center (the Center) to simulate radially varied

*A complete listing of references is given on page 56.

wake distribution for the cavitation experiment has been to use a so-called ring-type wake producer as shown in Figures 1a and 1b. Physically, this wake producer consists of many layers of concentric cylinders supported by four struts. The wake producer is installed upstream of the propeller plane, while the propeller is mounted downstream on the shaft of the tunnel. A typical velocity distribution along the circumferential planes at several propeller radii are given in Figure 2. The velocity was measured by a pitot tube and expressed in terms of column height of water. No control surface was included in the present test set-up. Owing to the presence of the four supporting struts, undesirable and complex crossflow patterns are generated at every junction of the concentric cylinder and the strut.[3] The complex crossflow patterns measured at the propeller plane are quite different from those measured on a ship hull with control surfaces. It is desirable to improve the flow field to conduct cavitation experiments.

Second, this approach fails to take into account the important effect of propeller-hull interaction on cavitation inception.

A third shortcoming associated with "Ring-Type Wake Simulator" is that shear flow around the propeller hub cannot be properly simulated. Hub vortex cavitation inception experiments will be subject to uncertainty.

The purpose of this program is to investigate the possibility of improving model propeller cavitation experiments so that cavitation performance of full-scale propellers can be predicted more reliably. The first phase of the program is to develop an improved method of simulating the radially varied inflow distribution at the propeller plane. To minimize the problems mentioned previously, the concept of "Semi-Geosim Ship Model" is introduced and developed.

This report presents the analytical and experimental results of using a semi-geosim model with mesh screens on the body surface to simulate a calculated full-scale wake (target wake) of an axisymmetric body. The wake simulation with a fully appended body and the corresponding cavitation tests of two large model propellers will be given in a separate report.

FULL-SCALE TARGET WAKE

Owing to the lack of measured full-scale data and to the difficulty of estimating corresponding wake analytically on a full-scale ship, previous cavitation experiments of a propeller model have been conducted under simulated wake conditions measured at the Reynolds number of the model. Owing to the two orders of magnitude of difference in Reynolds numbers between the model and a full-scale ship, it is known that the wake distributions under these two conditions will differ noticeably.[4] Different cavitation characteristics can be anticipated between model and full-scale propellers operated in different velocity fields. To increase accuracy in predicting cavitation inception of a full-scale propeller, wake distribution observed at a prototype should be simulated for the model propeller cavitation experiments.

Because measured full-scale data are lacking, the anticipated wake distribution at a prototype will be predicted analytically. The calculated wake is termed "full-scale target wake" and is to be simulated in the coming model propeller cavitation experiments. The procedure used to calculate the full-scale target wake and velocity profiles from a model ship will be briefly described.

CALCULATION PROCEDURE ON A BARE HULL

A single screw propeller operates within the stern boundary layer which arises from turbulent flow about the ship hull. As a result, the propeller blades experience a radially varied inflow velocity field. The mean axial velocity field $u(r/R_p)$, determined at the propeller plane without the propeller in place is called the nominal velocity distribution. Nominal wake fraction, $w(r/R_p)$ is defined by

$$1 - w(r/R_p) = u(r/R_p)/V \qquad (1)$$

where V = the ship speed

r = the radial distance from the shaft center of the propeller

R_p = the propeller radius

A potential flow and boundary-layer interaction program for axisymmetric bodies has been successfully developed at the Center.[5,6] The program uses a differential approach to solve the boundary-layer equations for a smooth bare hull and a displacement body approach to obtain the pressure distribution on the body. Experimental work[5] recently conducted at a Center wind tunnel showed the computed velocity profiles to be in good agreement with measured results for Reynolds numbers between 10^6 and 10^7.

ROUGH FULL-SCALE HULL

Calculating the full-scale wake on a rough hull presents a complex problem because the program is designed to make calculations on a smooth hull. The procedure currently in use at the Center is as follows. The effect of roughness is approximated by making the calculations at an equivalent Reynolds number R_{ne} which is lower than the actual full-scale Reynolds number R_{nf}. The reduction in Reynolds number is such that the resulting increase in overall skin friction C_F is equal to the observed increase ΔC_F due to roughness on the full-scale hull. The formula of the International Towing Tank Conference is used to obtain C_F at the full-scale Reynolds number R_{nf}.

$$C_F = \frac{0.075}{(\log_{10} R_{nf} - 2)^2} \tag{2}$$

Equation (2) is inverted to obtain the equivalent Reynolds number R_{ne} at the observed friction due to roughness, $C_F + \Delta C_F$

$$R_{ne} = 10^{\left(\sqrt{\frac{0.075}{C_F+\Delta C_F}} + 2\right)} = 100 \times 10^{\sqrt{\frac{0.075}{C_F+\Delta C_F}}} \tag{3}$$

The full-scale target wake is then taken to be the wake measured at model Reynolds number R_{nm} plus the difference between the computed wakes for R_{ne} and R_{nm}

$$\left(\frac{u}{V}\right)_f = \left(\frac{u}{V}\right)_m + \left[\left(\frac{u}{V}\right)_{R_{ne}} - \left(\frac{u}{V}\right)_{R_{nm}}\right]_c \qquad (4)$$

where u = velocity in the axial direction

V = speed of the model or full-scale body

f = full-scale target wake

m = measured values

c = calculated values

It is essential to use the measured model wake for appended hulls because the program does not at present account for appendages. For bare hulls, the requirement is less important since the predictions using the new version of the program are usually in good agreement with measured data at model R_n between 10^6 and 10^7. However, it should be noted that the program has not yet been explicitly validated at the higher R_n corresponding to R_{ne} and R_{nf} because experimental data are lacking.

TARGET WAKE OF A REPRESENTATIVE FULL-SCALE SHIP WITH APPENDAGES REMOVED

Figure 3 shows an axisymmetric body. This body has been extensively tested and compared between experimental and calculated velocity profiles for Reynolds numbers between 10^6 and 10^7; see References 5 and 6. This body, referred to as full-geosim body A, will be used to represent a typical full-scale ship hull with appendages removed. Corresponding offsets are given in Table 1. The velocity distribution at the propeller plane of this axisymmetric body as measured in a wind tunnel by Huang et al.[5] and Rood is given in Figure 4. Referring to Equation (4), let $\Delta u/V$ be defined as

$$\Delta u/V = \left(u/V\right)_{R_{ne}} - \left(u/V\right)_{R_{nm}} \qquad (5)$$

For assumed values of $R_{nf} = 2.0 \times 10^{9}$ and $\Delta C_F = 0.4 \times 10^{-3}$, the use of Equation (3) gives a value of $R_{ne} = 2.7 \times 10^{8}$. Table 2 shows the calculated values of $\Delta u/V$ at several radial distances from the center of the propeller shaft for $R_{nm} = 6 \times 10^{6}$ and $R_{ne} = 2.7 \times 10^{8}$. The target wake of full-geosim body A is constructed from the wake distribution measured at the model Reynolds number $(u/V)_m$ plus the correction term $\Delta u/V$ due to the difference in Reynolds numbers between the model and equivalent full-scale body. Figure 3 gives the computed target wake and the measured model wake. As expected, the boundary layer at the model Reynolds number is much thicker than that of the equivalent full-scale Reynolds number. The effect on the magnitude of the resultant inflow velocity due to $\Delta u/V$ is to change the angle of attack on the propeller blades.

The reliability of the computed target wake is a basic concern. The lack of measured full-scale data hampers the answer to this question. Nevertheless, recent studies at the Center strongly indicate that use of this computed target wake provides improved prediction as to full-scale propeller performances.

SEMI-GEOSIM SHIP MODEL

Local effects such as an isolated rough spot or deviation of geometric similarity, especially in the blade leading edge and the propeller tip areas, can alter markedly the critical cavitation inception indices. Unfortunately, the chord length associated with a typical model propeller is generally very small. Proper evaluation of the cavitation performance of a model propeller requires that as large a propeller as possible be tested so that the deviation in geometric similarity due to fabrication can be minimized. Reference 7 shows that cavitation inception indices can differ significantly between model and full-scale propellers due to the effect of pressure fluctuation in the boundary layer. Additionally, the propeller tip cavitation is known to be Reynolds number dependent. Minimization of the scale effect requires that the model propeller be tested at Reynolds numbers as large as possible. This, too, requires use of a large-sized

propeller as well as high speeds in water tunnel. These considerations indicate the advantages of using a large propeller and a large water tunnel with the capability to achieve high speeds. A propeller 18 in. (45.7 cm) in diameter was selected to be used for cavitation experiments in the 36-in. (91.4 cm) variable pressure water tunnel.

The represented full-geosim body A has a length-to-diameter ratio L/D = 10.97 with 44.2 percent of parallel middle body. The propeller plane is at x/L = 0.98, where x is the axial distance from the body nose. The ratio of propeller diameter D_p to maximum body diameter D is 0.545.

Figure 5 shows the 36-in. water tunnel and gives pertinent geometric dimensions. Figure 3 indicates that a full geosim of ship model required for an 18-in. (45.7 cm) propeller diameter would have a body diameter of 33.0 in. (84 cm) and a length of 30.25 ft (9.22 m). Both the body diameter and length would be intolerably large for the Center 36-in. water tunnel. Thus, it is clear that a body having much smaller diameter and length would have to be considered.

A propeller that is operating in close proximity to the ship hull afterbody and stern appendages acts to accelerate the flow in the stern boundary layer, giving rise to two propeller-hull-interaction effects: thrust deduction and modified nominal wake distribution, termed "effective wake distribution." To obtain reliable predictions of full-scale propeller cavitation performance, the two interaction effects must be included in the model propeller cavitation experiments. The computed results given in Reference 8 show that the significant contribution of thrust deduction is over the last 25 percent of the body length with 50 percent concentrated in the last 6 percent of the length. This length is slightly greater than one propeller diameter for the present body A.

To simulate the important effect of propeller-hull interaction on cavitation inception, the ship hull must be present. Selection of a 45.7 cm propeller as well as the constraints of tunnel walls led to a conflicting requirement in satisfying geometric similarity of the full-geosim ship hull and propeller. Recognizing that the major source of the propeller-hull interaction comes from the ship stern section and propeller, the concept of using a semi-geosim model for the cavitation test was introduced.

A semi-geosim body is defined as a ship model which satisfies the geometric similarity between the model and the prototype at the stern sections only.

Figure 6 shows the body aft of the parallel middle body section. It consists of a 0.305 m fifth-degree polynomial which fairs the parallel middle body to a 0.86 m stern. The polynomial satisfies continuity of radius, slope, and curvature at the upstream and downstream ends. The coefficients of the polynomial are also shown in Figure 6. A certain amount of trial and error was required to arrive at the proper length of the fairing. It was found that lengths less than 0.305 m led to bumps where the fairing had a radius exceeding that of the parallel middle body. This was due both to the requirement of meeting the geometric conditions on slope and curvature at both ends of the fairing and the difference of only 0.020 m between the radii at the upstream and downstream ends of the fairing. The last 0.86 m of the body is a geosim of the aft 9.3 percent of the stern of represented full-geosim body. The geosim was used in an attempt to preserve the pressure distribution and propeller and stern interaction on represented full-geosim body. As shown in Figure 6, the propeller is located 0.16 m forward of the tail.

Figure 2 shows a sketch of typical semi-geosim model. For comparison purposes, the represented full-geosim body is also shown. The model consists of a 0.61-m forward section fairing the tunnel shaft to a parallel middle body (PMB) section 0.46 cm in diameter ranging in length from 0 to 0.91 m, followed by the above described stern section.

As is the case of the aft fairing, the shape of the forward fairing is represented by a fifth-degree polynomial which satisfies continuity of radius, slope, and curvature at both ends. The length of 0.61 m was determined after some trial and error. Basically, the goal was to use as short a fairing as possible in order to minimize the overall length of the model so that it could be installed in the uniform test section. Calculations using the potential flow and boundary-layer interaction program indicated that a minimum of 0.61 m was needed to fair the shaft with radius 0.038 m to the parallel middle body with radius 0.23 m in order to avoid separation of flow. Figure 7 shows the forebody section.

While the shaft extends along the entire length of the water tunnel, it is necessary to terminate the front end of the shaft at a point in order to making computer runs using the potential flow and boundary-layer interaction program. For computer calculation purposes, the shaft forward of the fairing was somewhat arbitrarily extended to obtain a total body length of 3.66 m, regardless of the length of the PMB. The assumed bow is designated Bow 6 at the Center. It is a full bow with L/D = 1.82, surface area coefficient C_S = 0.909 and volume coefficient C_V = 0.850, where C_S and C_V are defined by

$$C_S = \frac{S}{\pi DL}$$

$$C_V = \frac{v}{\pi (D/2)^2 L}$$

where S is the surface area and v is the volume.
The length of shaft used was sufficient to insure that flow into the forward fairing was completely free of the stagnation effect from the assumed bow.

MODEL EXPERIMENTAL PROGRAM

EXPERIMENTAL PARAMETERS

Assume that the present semi-geosim model with a full geosim stern afterbody and a mathematical forebody is adequate for propeller-hull interaction. Simulating most of the effect of the intolerable demand on geometric similarity of the ship hull is circumvented. Thus, the effective wake distribution is simulated if the nominal wake distributions (velocity field) are similar between the semi-geosim model and the prototype.

Successful installation of the model imposed by the tunnel walls limits the maximum allowable body diameter to 45.7 cm. As seen in Figure 3 the wake distributions between the present semi-geosim model and the full-geosim body A are likely to differ because of the significant difference

in the body shapes. The purpose of present experimental program is to develop a method to better simulate the target wake of full-scale ship by using a semi-geosim ship model with various combinations of parallel middle body length and mesh screens installed on the body surface.

MODEL DESCRIPTION

References 9 and 10 show that a mesh screen installed on a body surface can be used effectively to enhance development of turbulent boundary layers. Work by Cebeci and Smith[11] shows that it is necessary to treat a turbulent boundary layer as a composite of an inner and an outer region. When a mesh screen is placed on the body surface in a turbulent boundary layer, the effect of disturbance in the inner region disappears in a relatively short distance because of the highly diffuse nature of the flow. The inner part of the velocity profile returns more quickly to a normal profile shape than does the outer part. Experimental work by Robbins[10] also indicates that it is more effective to influence and enhance development of the turbulent boundary layer by installing the surface screens far upstream from the propeller plane.

The semi-geosim model with a 0.91 m parallel middle body (PMB) is shown in Figure 8. The model is made of fiberglass. The PMB is made of two pieces with equal length (0.47 m) and can be removed from the body to investigate the effect of PMB on wake distribution. Body roughness is simulated by installing mesh screens on the body surface. They are located at the fore and parallel middle bodies and can be arranged in various combinations in length and location. The consideration given in the selection of mesh size is to avoid the occurrence of cavitation on the surface screen within the range of cavitation numbers to be examined in the future propeller cavitation tests.

Table 3 gives results of investigating nine configurations of the model in the 36-in. water tunnel. Configuration 1 consists of a fore and an aft body. Configuration 2 includes a 0.46 m parallel middle body. Mesh screen Type I corresponds to mesh size 10. The wire is 0.063 cm in diameter with mesh spacing of 10 wires per 2.54 cm. The open area is 56.3

percent. Mesh screen Type II also corresponds to mesh size 10. However, the wire is 0.08 cm in diameter with mesh spacing of 10 wires per 2.54 cm. The open area is 46.2 percent. To take advantage of available space, an additional 1.83 m in length of mesh screen Type I was placed in several model configurations at the water tunnel shaft housing ahead of the semi-geosim model.

Experiments with the model were conducted in the 36-in. variable pressure water tunnel. To minimize the possible effect of the tunnel wall on the propeller performance, the free-jet test section was used. The model was mounted on the tunnel shaft housing. Figure 9 shows the model in a test condition; the major part of the body is inside of the tunnel, and part of the stern section is visible in the free-jet section.

A wake rake fitted with six five-hole pitot tubes was used to measure the magnitude and direction of the inflow velocity. The pitot tubes were 0.95 cm in diameter and were located on the propeller plane, 6.86, 9.14, 11.4, 16.0, 20.57, and 24.0 cm away from the center of the shaft. For a propeller 45.7 cm in diameter, they corresponded to r/R_p = 0.3, 0.4, 0.5, 0.7, 0.9, and 1.05, respectively. The symbol r denotes the radial distance from the center of the shaft and R_p denotes the propeller radius. The shaft could be rotated manually to measure the velocity distribution on the circumferential plane.

EXPERIMENTAL RESULTS

The velocity component in the axial direction is much greater than in the radial direction. Consequently, only the axial component is given in this report. The shaft was rotated manually at every 18-deg intervals to obtain the circumferential mean velocity. The wake survey was carried out at the tunnel pressure of 138 kPa for all configurations. Tables 4 and 5 give results of the experiment. The effect of the variation in tunnel shape should be noted in comparing the test data.

BARE HULL: CONFIGURATIONS 1 AND 2

Configurations 1 and 2 consist of fore and aft bodies with 0 and 0.46 m PMB's, respectively. The measured velocity distributions of these two

configurations are given in Figure 10. Significant wake defects are observed only in the propeller inner region. The flow was almost uniform in the outer region $r/R_p \geq 0.6$. The results were due to the fact that relative to propeller diameter the semi-geosim model was small in size, compared to the represented full-geosim body shown in Figure 3.

The theoretically computed velocity profile at $R_n = 4.6 \times 10^7$, corresponding to a free-stream velocity of 11.58 m/s are also given in the same figure for comparison. The theory is based on an infinite fluid condition. Strictly speaking, direct comparison between measured data from a water tunnel and calculated results, based on an infinite fluid theory, seems improper. Nevertheless, the velocity distributions measured and computed do exhibit similar trends. The measured increment in the wake defect due to adding 0.46 m of PMB does agree qualitatively with predicted results. The measured velocity profiles in the inner region exhibited much stronger wake defects than did those calculated.

The pressure distributions on the body surface of Configuration 2 placed in the 36-in. water tunnel versus an infinite fluid were computed by Bai, based on a potential flow theory.[12] The water tunnel downstream of the experimental section was idealized by assuming a uniform cross section. Figure 11 gives computed results. Note that the pressure coefficient C_p given in the figure was normalized by using the downstream velocity V_d and

$$C_P = \frac{P-P_d}{1/2\rho V_d^2}$$

where P = local pressure

P_d = pressure far downstream

ρ = fluid density

The trends between the two computed pressure distributions are similar. Nevertheless, the magnitudes and pressure gradients are significantly stronger with the model in the water tunnel than in an infinite fluid. Figure 11 shows that a further improvement in model design and prediction

of velocity and pressure distributions can be obtained if the Bai potential flow theory with finite-flow boundaries could be extended to the boundary-layer computation.

MESH SCREENS ON BODY SURFACE: CONFIGURATIONS 3 THROUGH 6

To take advantage of available space, 1.83-m long mesh screen of Type I was installed at the shaft housing ahead of the model on Configurations 3 through 5. The basic body shapes of Configurations 3 through 5 were the same as the shape of Configuration 2. Type I surface screens of 22.9, 45.7, and 68.6 cm were placed on the body at location A, locations A and B, and locations A, B, and C to form Configurations 3 through 5, respectively; see Figure 8. The 1.83-m mesh screen installed at the shaft housing ahead of the model was removed from Configuration 5 to form Configuration 6.

The measured velocity distributions will now be expressed in dimensionless forms for comparison with the full-scale target wake to be simulated. Referring to Figure 5, the tunnel configuration is seen to vary almost continuously. There is no unique way to define the upstream velocity. Note that conducting the propeller cavitation tests only requires knowing the velocity field at the propeller plane. The measured velocity profiles can be used as input to a propeller prediction computer program to determine the corresponding free-stream velocity at a given thrust coefficient K_T and an advance ratio J. For the present work the following approach has been taken. Development of turbulent boundary layers at various configurations can be studied and compared by normalizing the velocity in such a way that the velocity ratios are equal to 0.80 for all configurations at $r/R_p = 0.9$ (pitot tube 5). The dimensionless velocity profiles for Configurations 2 through 6 are given in Figure 12.

Effectiveness of the surface screens on development of a thicker turbulent boundary layer is clearly demonstrated. The wake defect with installation of a surface screen now extends to r/R_p of approximately 0.7 to 0.8 compared to a value of 0.5 to 0.6 without surface screens. In the outer radii, say that $r/R_p > 0.8$, the flows still remain almost uniform

while the wind tunnel wake and target wake still exhibit significant wake defect. A comparison of measured velocity profiles for Configurations 5 and 6 indicates that the effectiveness of a 1.83 m surface screen placed on the shaft housing ahead of the model is only marginal. This is due partly to an extremely low velocity, associated with the large tunnel cross section, and partly to the very small surface area, associated with the small shaft-housing diameter, compared to the model body diameter.

HEAVY MESH SCREEN: CONFIGURATION 7

To investigate the effect of mesh size on the velocity profile, a layer of mesh screen Type II was placed on top of mesh screen Type I of Configuration 4 to form Configuration 7. Additionally a slight difference exists between Configurations 4 and 7. There was no surface screen on the shaft housing for Configuration 7. Figure 13 gives the measured velocity distributions of these two configurations. Within the accuracy of measurements, the two measured velocity distributions are almost identical.

EXTRA PARALLEL MIDDLE BODY: CONFIGURATION 8

Additional 0.46 m of PMB was added to Configuration 6 to form Configuration 8. In this configuration the forward part of the model was extended to a much expanded region of tunnel cross section, resulting in more and greater hydrostatic drag. To ensure the safety of structural supports on the model, Configurations 8 and 9 were tested at reduced speeds. Figure 14 gives the velocity profiles of these two configurations. The additional 0.46 m of PMB actually produced less wake defect, which may be explained by referring to Figure 5. An additional 0.46 m of PMB is seen to push the forebody, located in a nearly uniform test cross section, into an expanded cross section. The flow passes through the forebody of Configuration 8, which is thus slower than that of Configuration 6. Without the available theoretical computations, this reasoning can only be viewed as a plausible explanation.

EXTRA LENGTH OF MESH SCREEN: CONFIGURATION 9

An additional surface screen D of 0.46 m was installed on PMB of Configuration 8 to form Configuration 9; see Figure 8. The corresponding velocity distribution is given in Figure 14. The effectiveness of surface screen D to enhance the wake defect is seen by comparing measured velocities between Configurations 8 and 9. The measured velocities of Configuration 9 are almost the same as those of Configuration 6.

BRIEF DISCUSSION

Figure 12 shows that mesh screens installed on the body surface are very effective in modifying the velocity profiles. It also shows that the measured velocity defect with the present model only reaches from r = 16.0 to 18.3 cm from the center of the shaft, corresponding to r/R_p = 0.7 ~ 0.8 for a 45.7 cm propeller. Because of the relatively short and thin model as compared to the full-geosim body (Figure 3), the measured velocity ratio of Configuration 4 differs 6 to 8 percent from the desired target wake distribution in the tip for a 45.7 cm propeller.

It is known that a so-called ring-type wake producer can provide a wake defect in the outer radii. However, care must be exercised in terms of the undesirable cross flow associated with the ring-type wake producer. One thing in favor of this approach is that a significant amount of wake defect has already been generated by the semi-geosim body. It will require fewer concentric cylindrical plates to generate the remaining wake defect. Owing budgetary constraints, this device attached on a semi-geosim model has not been investigated.

WAKE DISTRIBUTIONS VERSUS MODEL PROPELLER SIZES

Figure 12 shows that the measured velocity defect with the present semi-geosim model can reach r = 18 cm from the center of the shaft, which is at the tip of a 35.6 cm propeller. The feasibility of using a 35.6 cm propeller for cavitation tests will be discussed. The stern section of the present semi-geosim model is based on the length scale of a 45.7 cm propeller fitted on the full-geosim body. Using a 35.6 cm propeller would

require construction of a new stern section and a new series of wake surveys. Figure 3 shows that the stern section is close to a wedge shape. This means that the deviation in geometric similarity of stern sections associated with length scales of 35.6 - and 45.7 cm will be small. To minimize the cost, and as a first approximation the following plausible approach is used for this investigation.

For the present semi-geosim model, the plane of a 35.6 cm propeller will be located approximately 3.5 cm behind the plane of a 45.7 cm propeller. Locating a propeller plane is based on the requirement that the propeller hub radius r_h equal 0.21 R_p. It is assumed that the difference in velocity distributions at 3.5 cm intervals along the radius length between the two propeller planes is small and negligible. Namely, the velocity distributions $u(r-r_h)$ are assumed to be the same between the two propeller planes. Measured velocity distributions along the radial distance as given in Figure 12 and Table 4 will be used for a 35.6 cm propeller study. Extrapolated velocity distributions along the propeller plane for various model configurations are given in Table 6. The measured velocities given in Table 4 remain the same. However, the corresponding radial distance $\bar{r}$ for a 35.6 cm propeller has been corrected.

For purposes of discussion, the measured velocities at $\bar{r}/R_p = 1.10$ (pitot tube 5) are normalized to 0.87 for all configurations; see Table 7. Velocity distributions associated with Configurations 3 through 5 are given in Figure 15. The wake defect now reaches to the propeller tip. The velocity distribution associated with Configuration 4 is seen to fit the full-scale target wake reasonably well.

TUNNEL SPEED EFFECT ON WAKE DISTRIBUTION

The same semi-geosim model was investigated at different tunnel speeds to determine the possible effect of speed on velocity distribution. The tunnel velocity in this series of tests was approximately one-half of the velocity used in the previous experiments. The wake survey was carried out at the same tunnel pressure of 138 kPa, the same value used previously. Observe that the cavitation number in these experiments is approximately 4 times higher than that of the previous series. The measured velocities at various radial distances for several model configurations are given in Tables 8 and 9.

Simply stated, the tunnel velocity associated with the experiments given in Table 4 is referred to as the "high-velocity series." The tunnel velocity associated with the present series given in Tables 8 and 9 is referred to as the "low-velocity series." Corresponding velocity distributions are given in Figures 16a, 16b, and 16c for Configurations 2, 4, and 5, respectively. The measured velocity distributions for the two series exhibit only very slight differences, which is not a surprise as the difference in Reynolds numbers between the two series is only a factor of 2. Within the variations of a factor of two in tunnel speeds and a factor of 4 in cavitation numbers, the velocity profiles may be considered to be essentially similar.

WAKE SIMULATION WITH FULL APPENDAGES

Model wake and full scale target wake of a ship with appendages are given in Figure 17.* The numerical value given here corresponds to the correlation allowance of $C_A = 0.25 \times 10^{-3}$. The theoretical computation so far embodies the assumption that the effect of appendages on the nominal velocity distribution is independent of Reynolds number.

The semi-geosim model with stern appendages is given in Figure 18. The model is fitted with the parallel midbody of 0.46 meters. Wake simulation with full appendages was conducted 6 months later from the bare hull work. A new configuration number was assigned to this series of tests. To be consistent with the data in the file, these new model configuration numbers are preserved. For example, aside from the stern appendages, Model Configuration I in full appendage study is the same as Model Configuration II in Bare hull study; see Tables 3 and 10.

The measured circumferentially averaged velocities in the axial component are given in Tables 10 and 11, and plotted in Figure 19 for $D_p = 45.7$ cm. The measured velocities have been normalized in such a way that the velocity ratios are equal to 0.80 at $r/R_p = 0.9$ (Pitot tube 5) for all model configurations. This choice is based on the idea that the measured velocity distribution matches the target wake closely around r/R_p from 0.5 to 0.8. Obviously, the choice of this reference velocity is subjective. A further discussion on this subject is discussed by Shen et. al.**

Similar to the result shown in Figure 12 for the bare hull condition, the wake defects only reach r/R_p around 0.7 to 0.8 for a 45.7 cm propeller. In the outer radii, say $r/R_p > 0.8$, the flows remain almost uniform. A deviation of 6 percent in the velocity ratio at the propellers tip is noticed between measured and target wakes. Following the similar approach given in the bare hull, the extrapolated velocity distributions along the propeller plane for a 35.6 cm propeller are given in Tables 12 and 13, and plotted in Figure 20 for various model configurations. The wake defect

---

* Rood, E.P., Unpublished Report
* West, E.E., Unpublished Report
* Grant, J.W., Unpublished Report
** Shen et al Unpublished Report

now reaches to the propeller tip. Circumferentially averaged velocity distribution associated with Configuration 5 is seen to fit the full-scale target wake reasonably well. The measured local velocity distributions along the circumferential planes for Configuration 5 are given in Figure 21a at $\bar{r}/R_p$= 1.29, 1.09 and 0.84, and in Figure 21b at $\bar{r}/R_p$= 0.58, 0.45 and 0.32. The vertical axis gives the velocity ratio and the horizontal axis gives the polar angle along the circumferential plane. The zero polar angle is aligned with the vertical axis at 12 o'clock direction.

The local velocity distributions along the circumferential planes on a full-geosim model conducted in a wind tunnel* were also shown in Figures 21a and 21 b for comparison. The wake survey by Rood* was conducted in different propeller radii. Consequently, in some of the figures the measured wind tunnel velocity distributions at two different propeller radii are shown in the same plot with velocity distribution measured in the present model. As an example, the measured velocity distributions in the wind tunnel at r/R_p= 0.953 and 0.75 are shown in the same plot with the velocity distribution measured at r/R_p= 0.84 for the current model.

The current model is intended to simulate a full-scale target wake. As seen in Figure 20, the velocity ratios in the present model should be higher than those measured in the wind tunnel by the amount of $\frac{\Delta u(r)}{V}$. In general, the measured circumferential wake distribution using the present semi-geosim ship model gives velocity fluctuations behind the appendages similar to those measured in the wind tunnel with a full-geosim model. In summary, the wake field to be anticipated in a full-scale ship appears to be produced by the present ship model to within a few percent for a 14-inch model propeller.

---

* Rood, E.P., Unpublished Report

CONCLUDING REMARK

Experimental results measured in the 36-inch water tunnel indicate that the target wake of a represented full-scale ship can be reasonably simulated up to the propeller tip by the present semi-geosim model with a propeller 14 in. (35.6 cm) in diameter. A deviation of 6 percent in velocity ratio at the propeller tip from the target wake may be encountered if an 18-in. (46.5 cm) model propeller is used along with the present semi-geosim model. A possible means to improve wake simulation is suggested in the text if a large size propeller is to be used.

It is expected that the important effect of propeller hull interaction on propeller cavitation can be reasonably incorporated by the use of a semi-geosim ship model. The use of this model also eliminates the undesirable complex cross-flow patterns into the propeller disk as observed with the ring-type wake producer. Additionally, a simulated shear flow around the propeller hub is expected to improve hub vortex cavitation inception experiments.

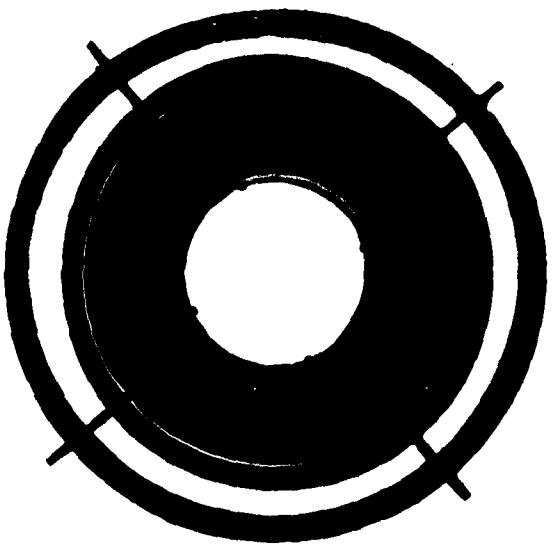

Figure 1a - Front View of a Ring Type Wake Producer

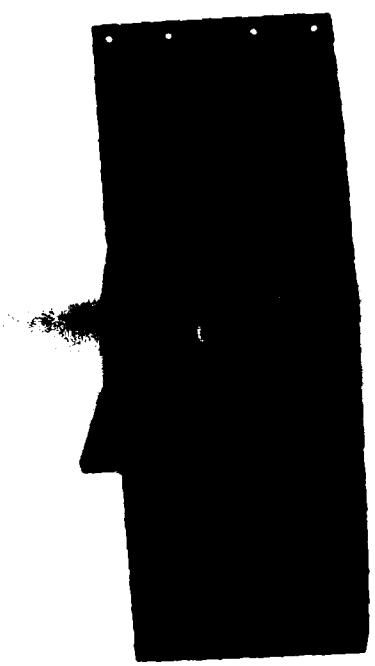

Figure 1b -Side View of a Ring Type Wake Producer

Figure 1 - Ring Type Wake Producer

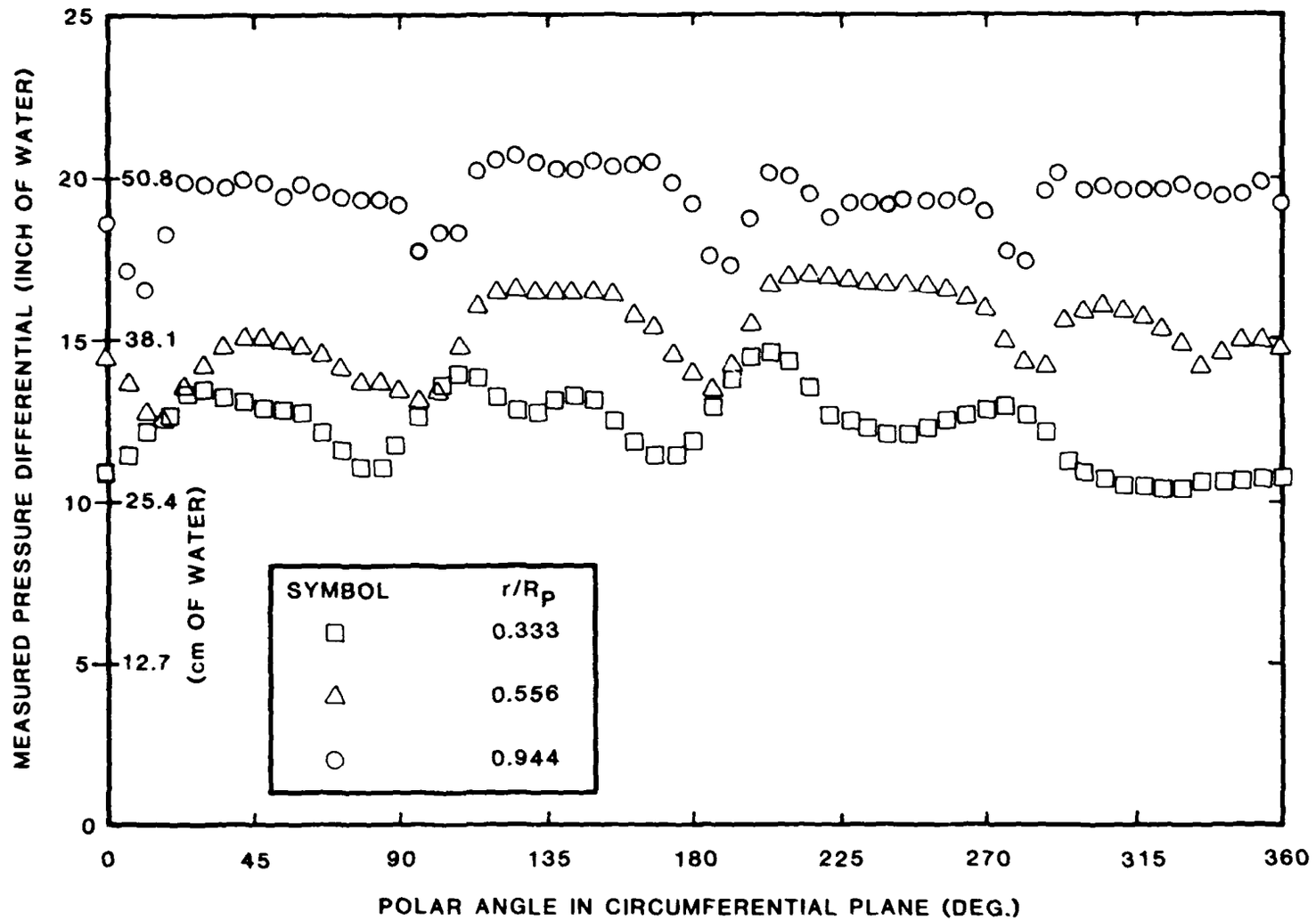

Figure 2 - Velocity Variation in Circumferential Planes Generated by "Ring Type Wake Producer" (No Control Surfaces)

PRECEDING PAGE BLANK-NOT FILMED

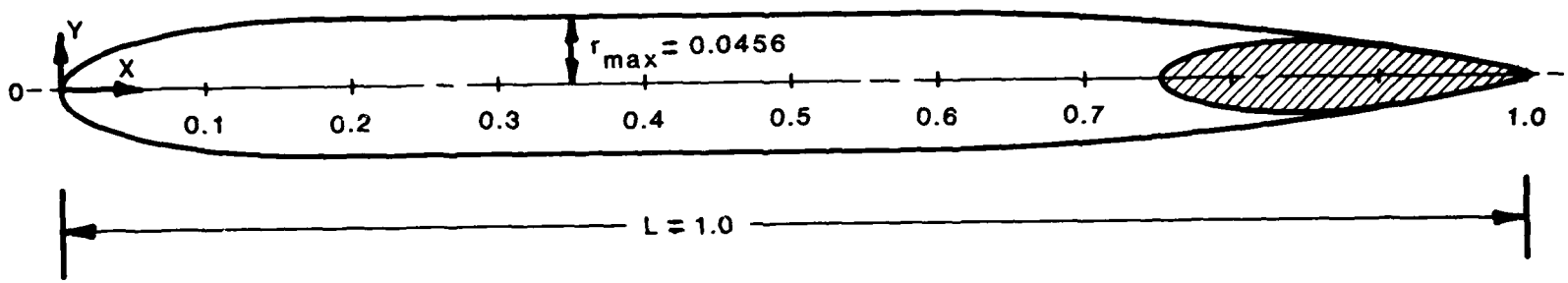

Figure 3 - The Represented Full-Geosim Body and Present Semi-Geosim Model

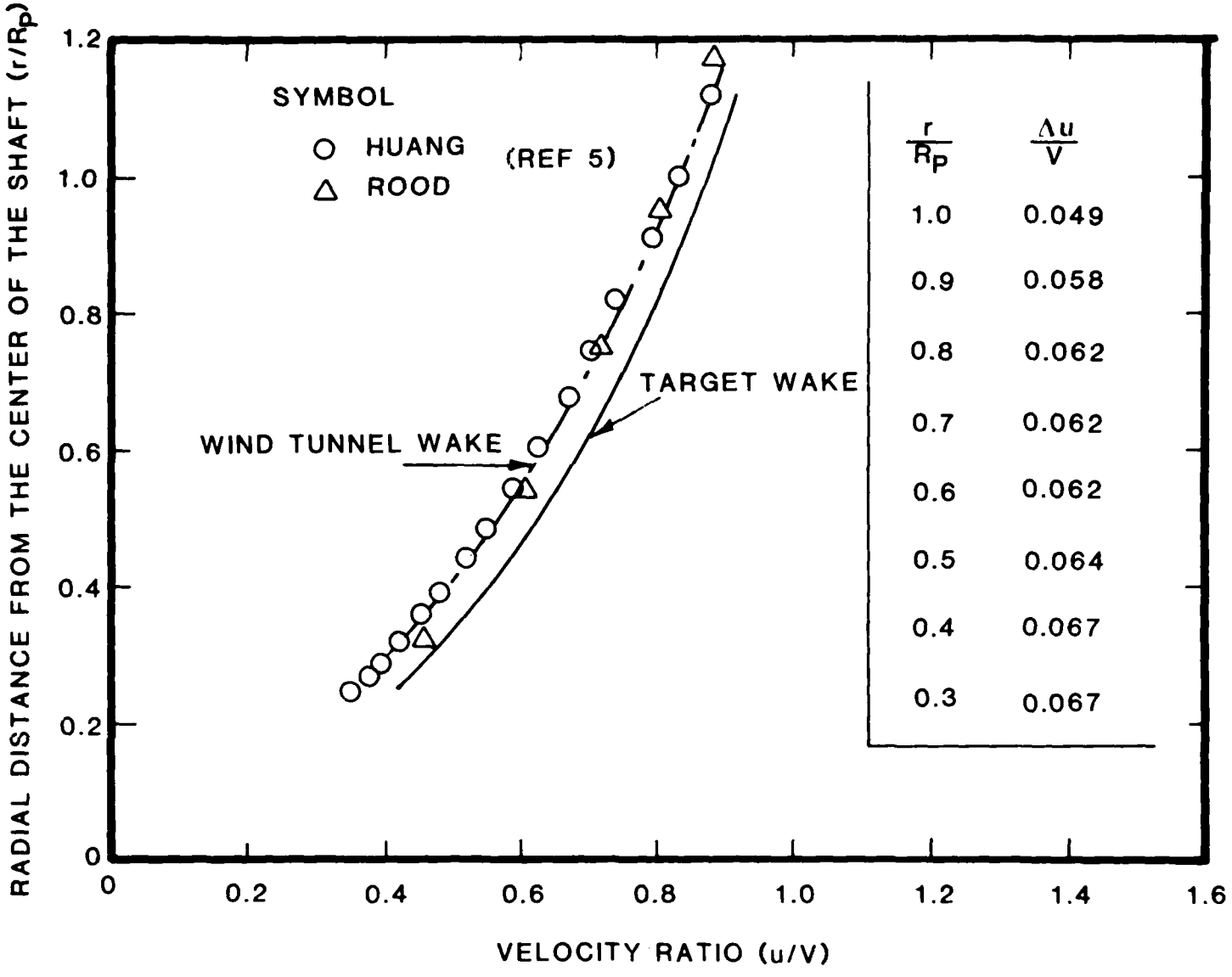

Figure 4 - Measured Wind Tunnel Wake and Computed Target Wake

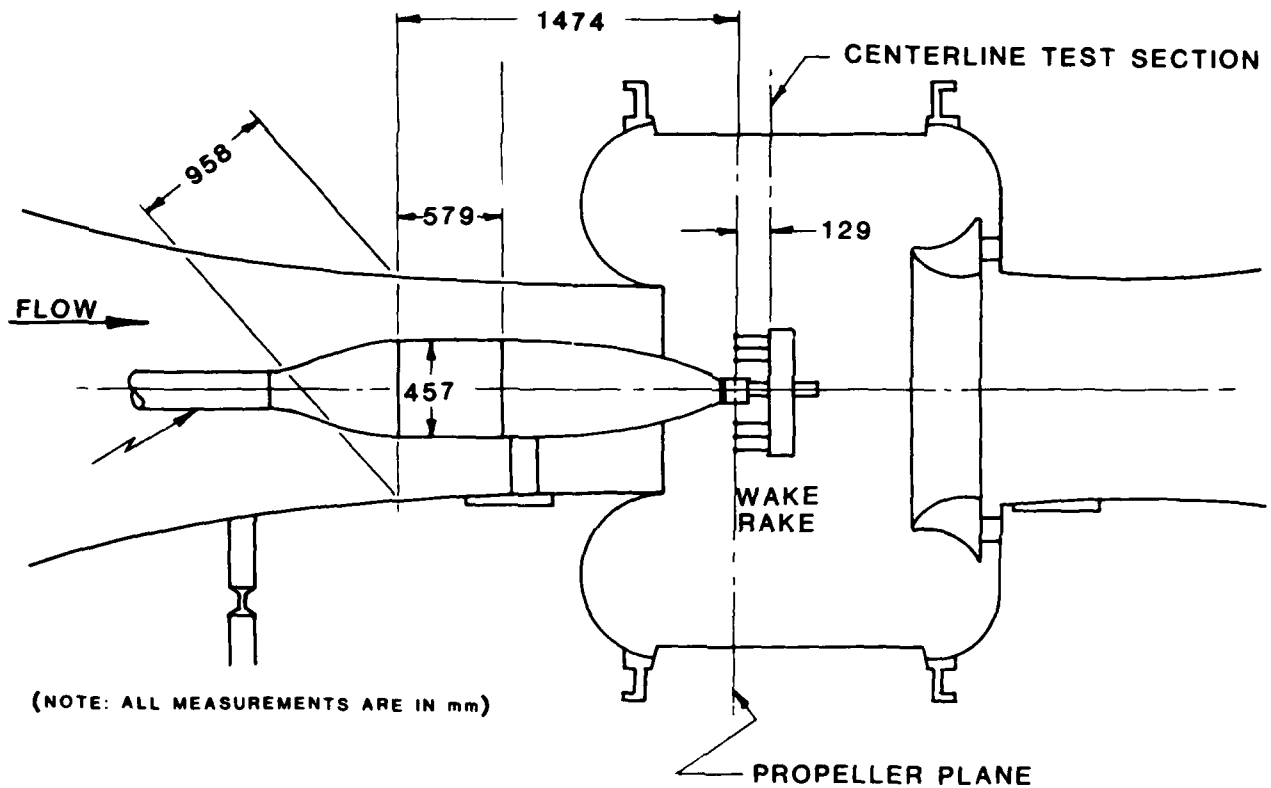

Figure 5 - Thirty-Six Inch Water Tunnel and the Present Model

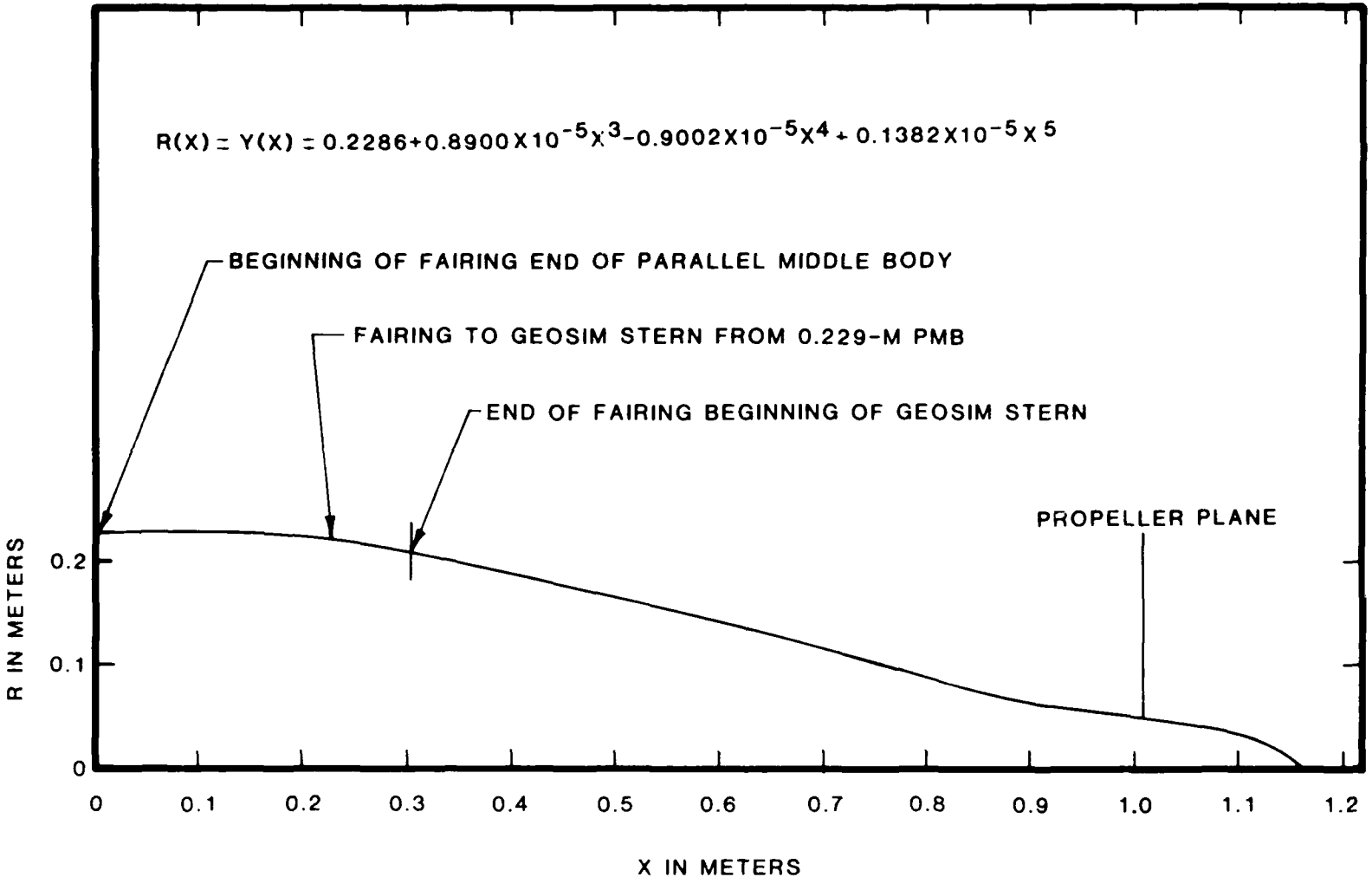

Figure 6 - Sketch of Test Body Aft of Parallel Middle Body Section

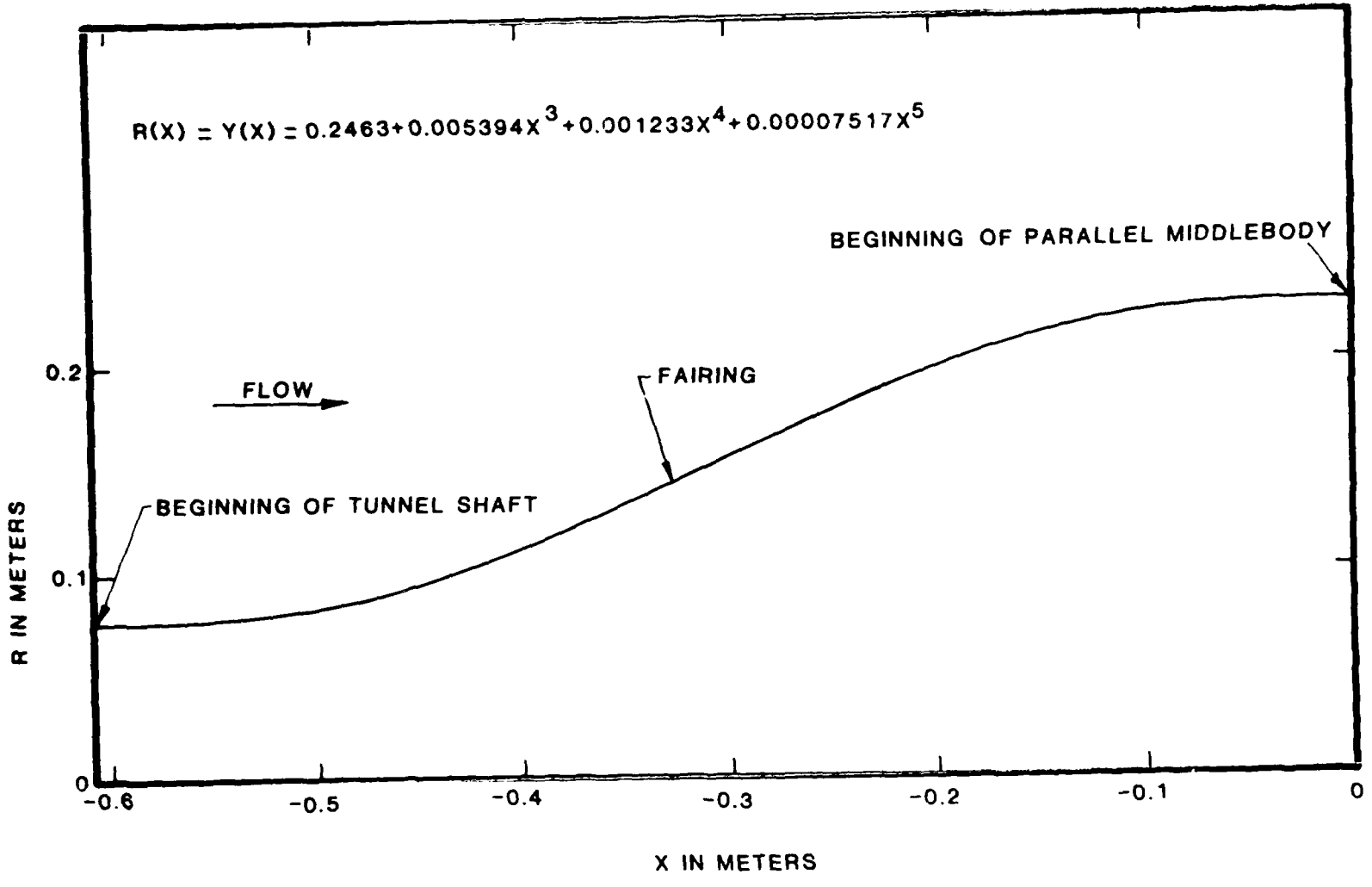

Figure 7 - Sketch of 0.61-M Forward Fairing From Tunnel Shaft to Parallel Middle Body

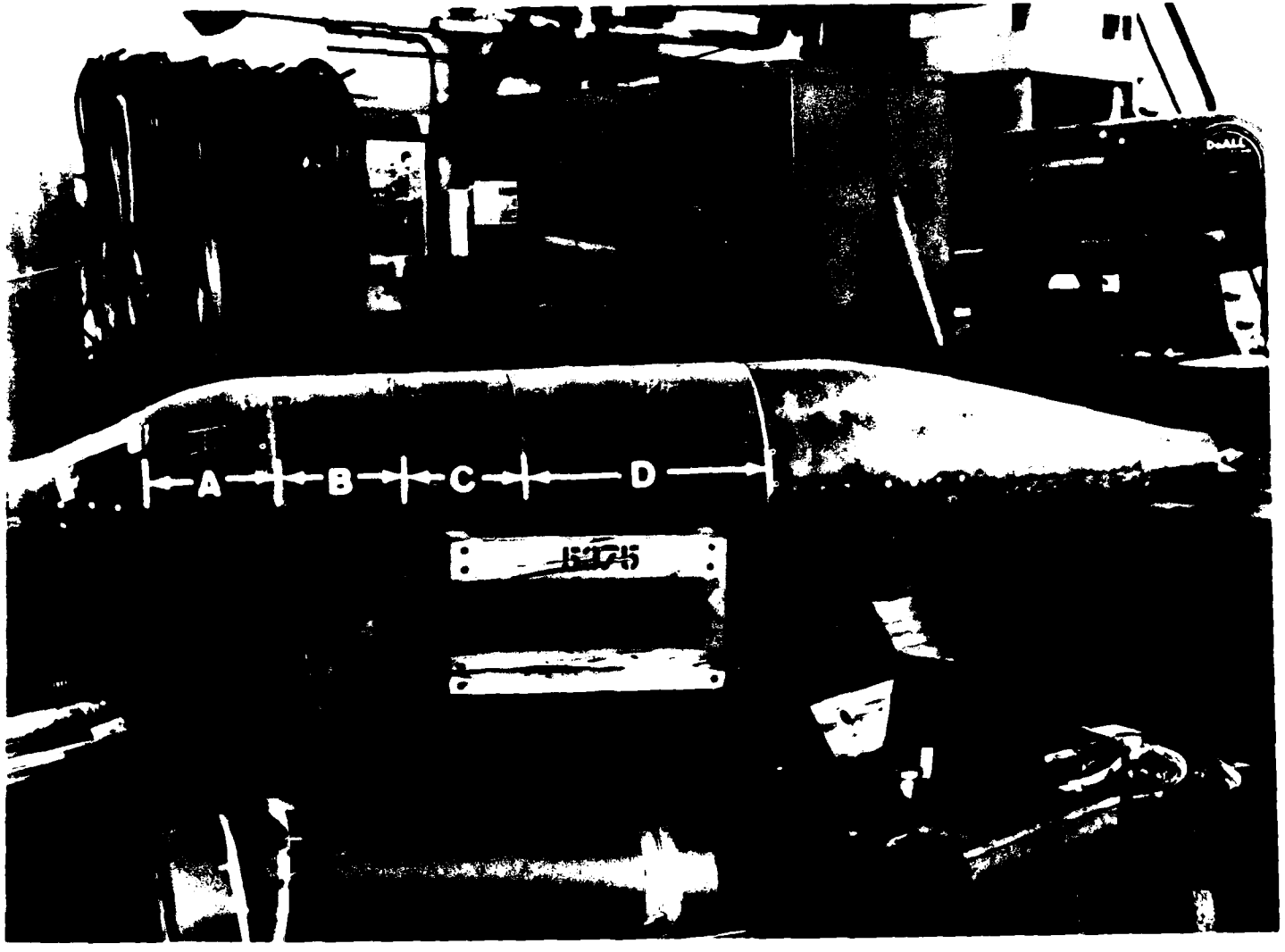

Figure 8 - Semi-Geosim Ship Model

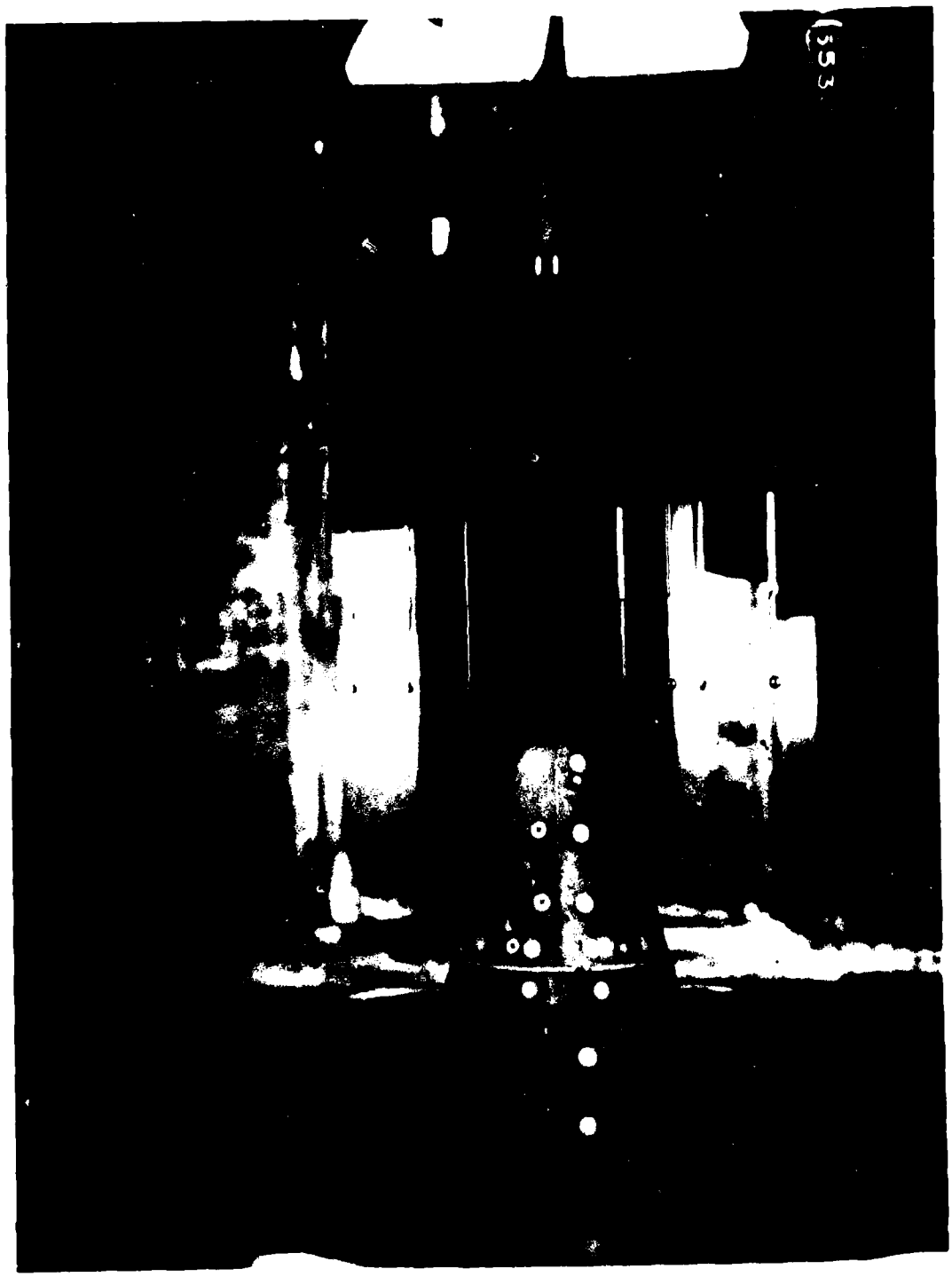

Figure 9 - Model and Wake Rake in Thirty-Six-Inch Water Tunnel Open Jet Test Section

PRECEDING PAGE BLANK-NOT FILMED

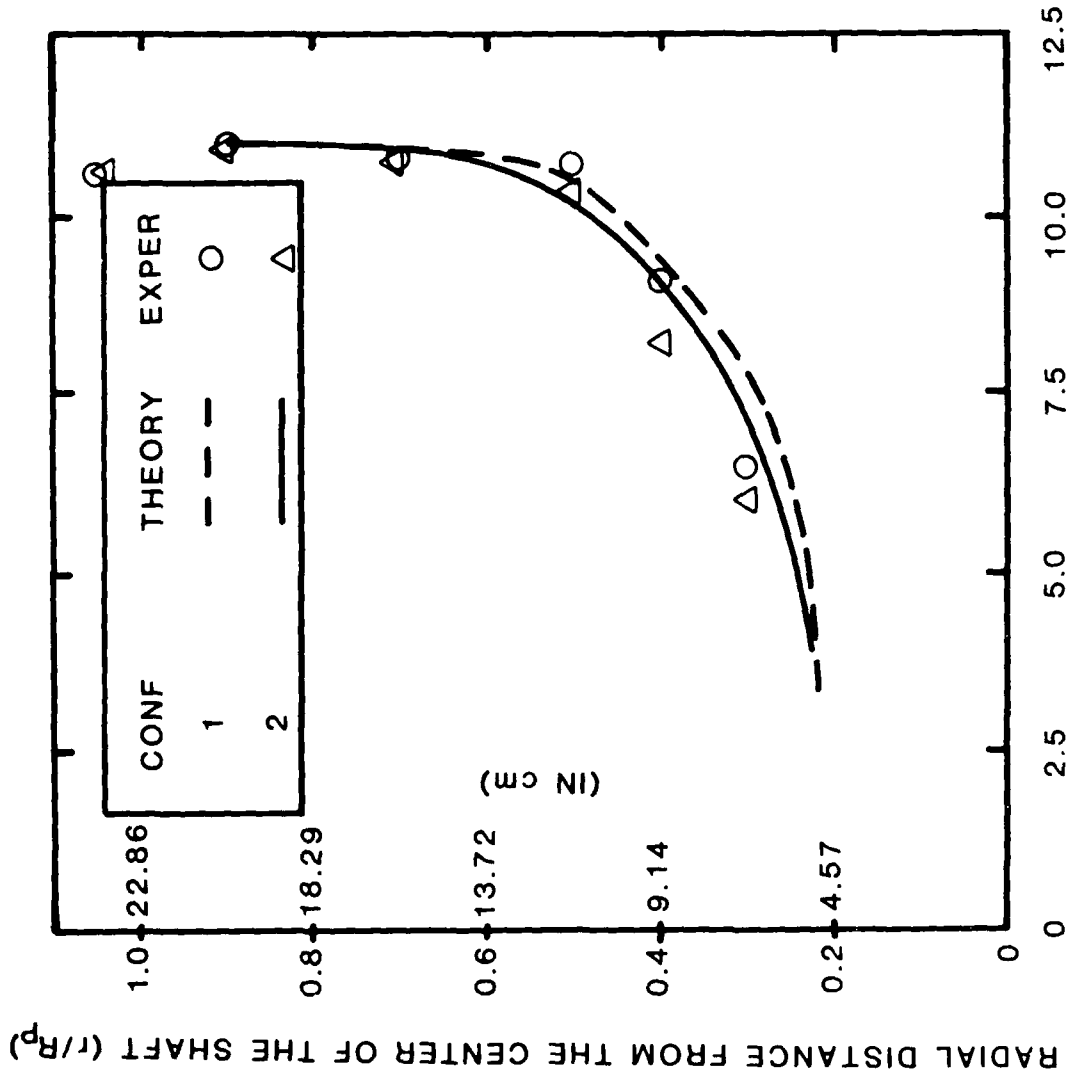

Figure 14 - Measured Velocity Distributions for Model Configurations 1 and 2

PRECEDING PAGE BLANK-NOT FILMED

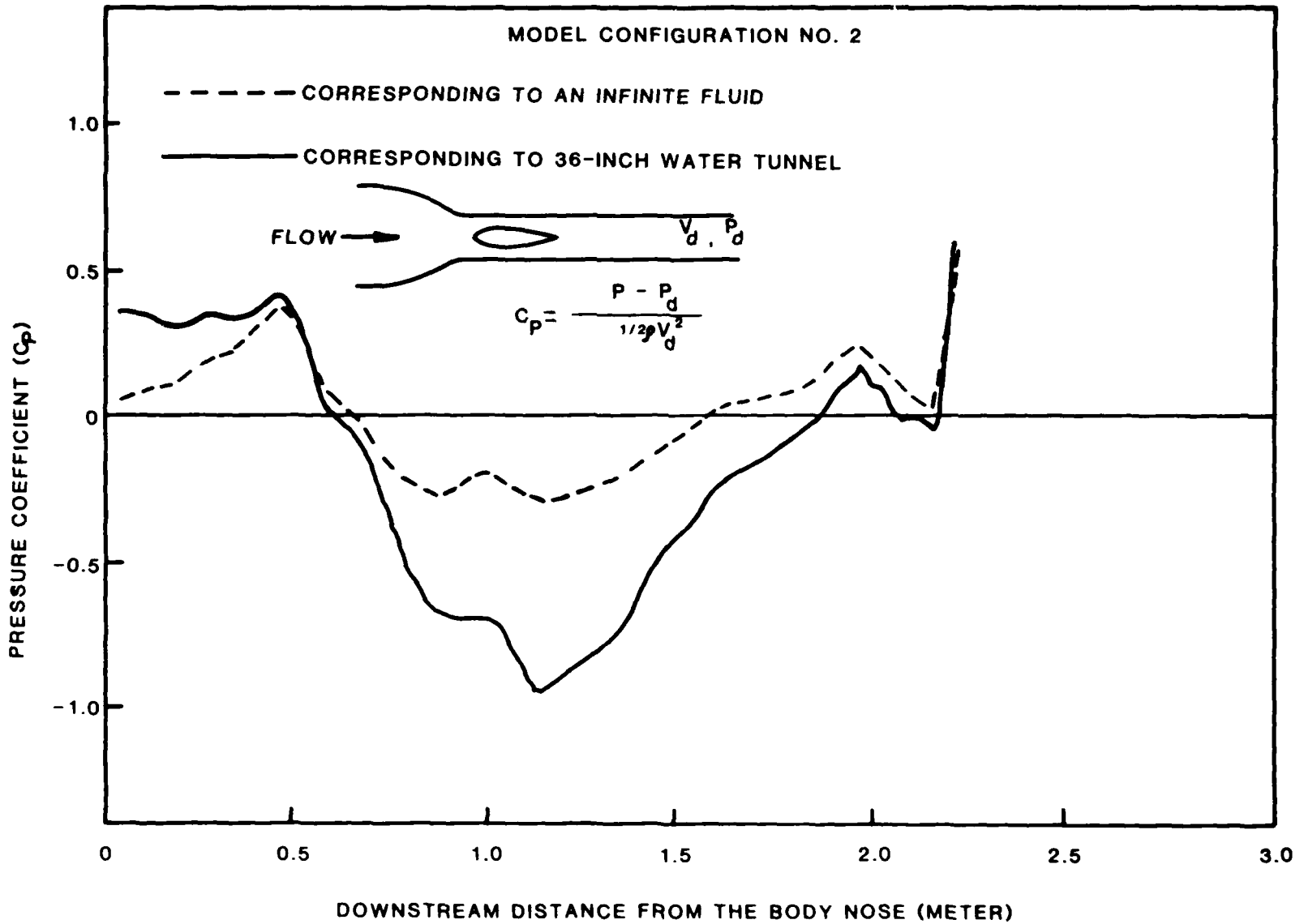

Figure 11 - A Comparison of Calculated Pressure Distributions on the Body Surface in an Infinite Fluid and Thirty-Six Inch Water Tunnel

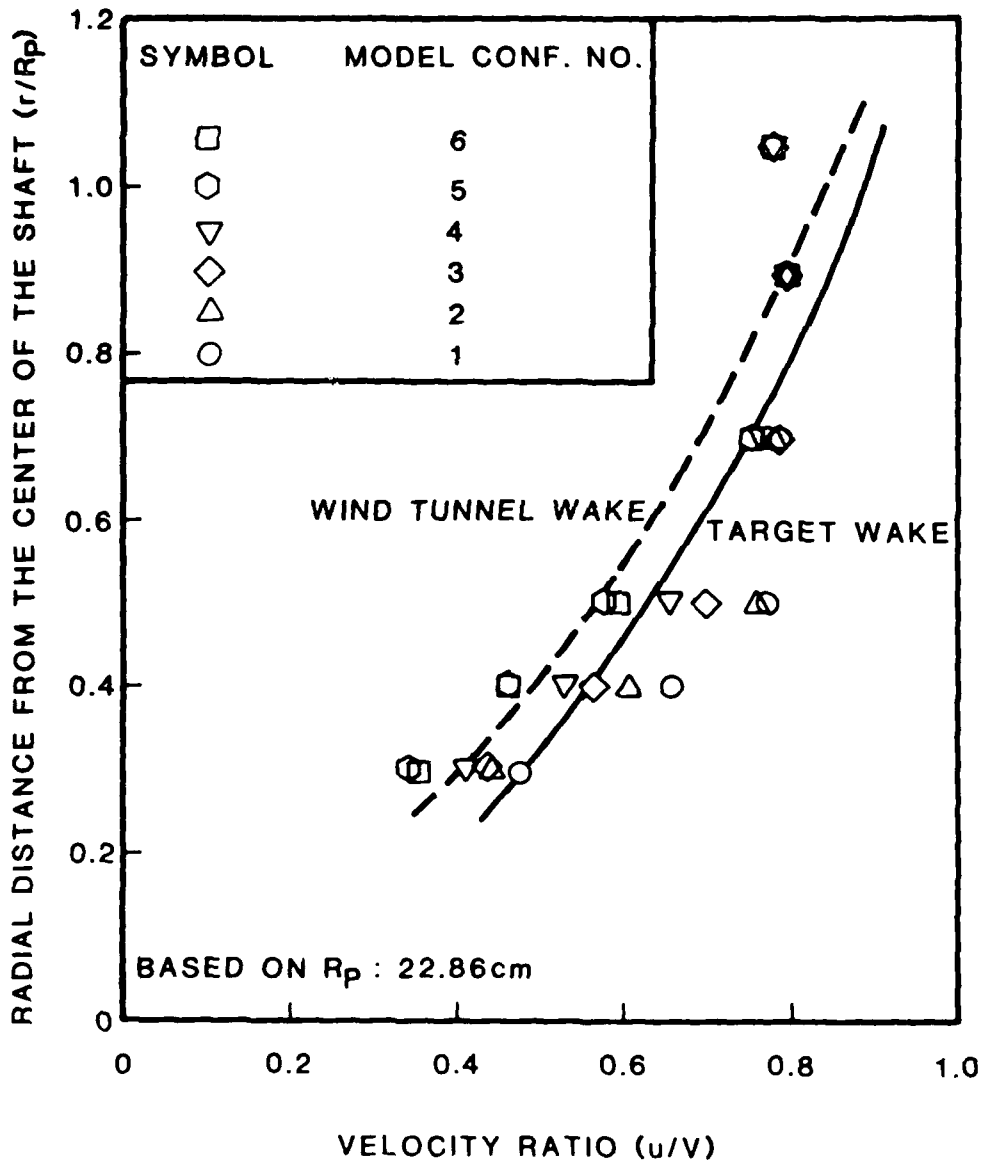

Figure 12 - Measured Velocity Distributions of Model Configurations 1 and 6

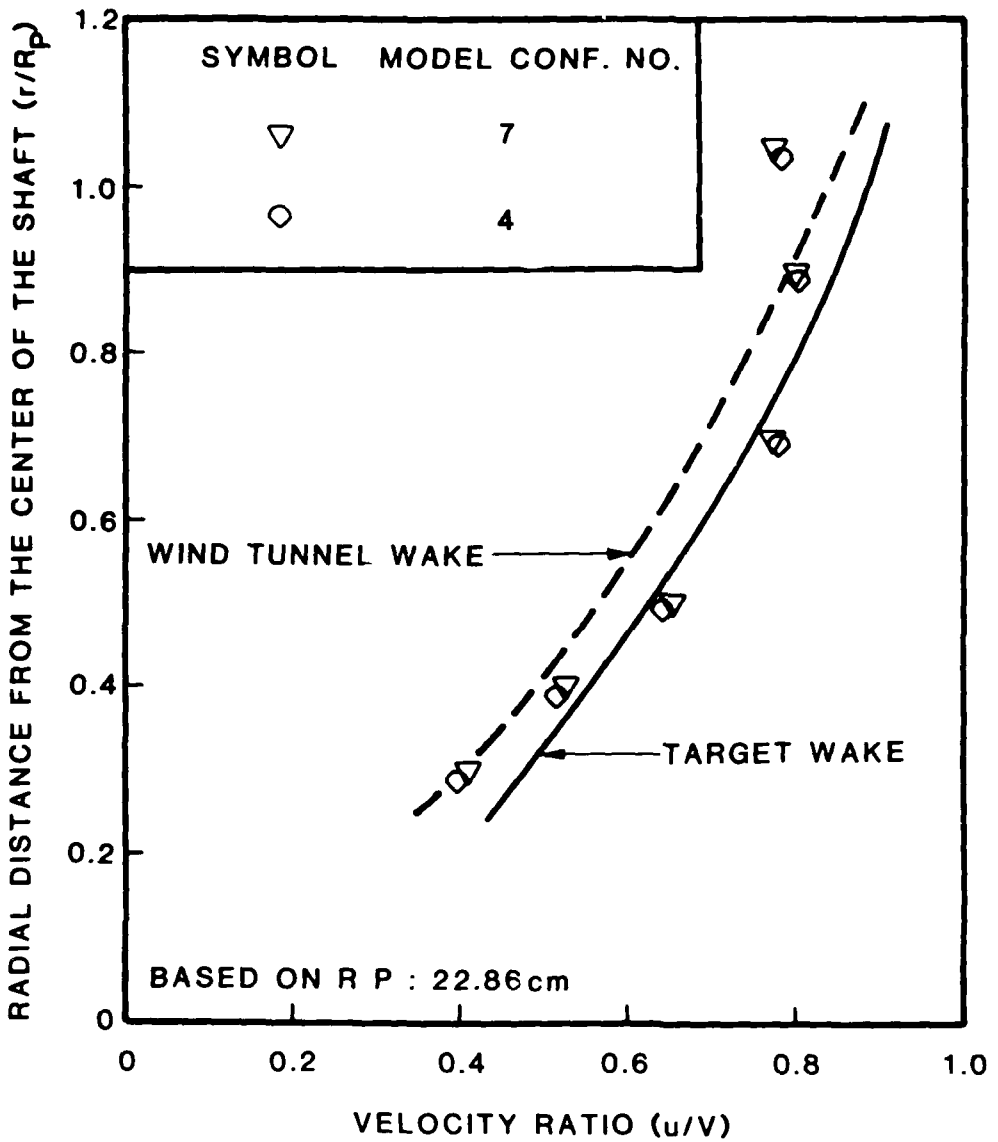

Figure 13 - Measured Velocity Distributions of Model Configurations 4 and 7

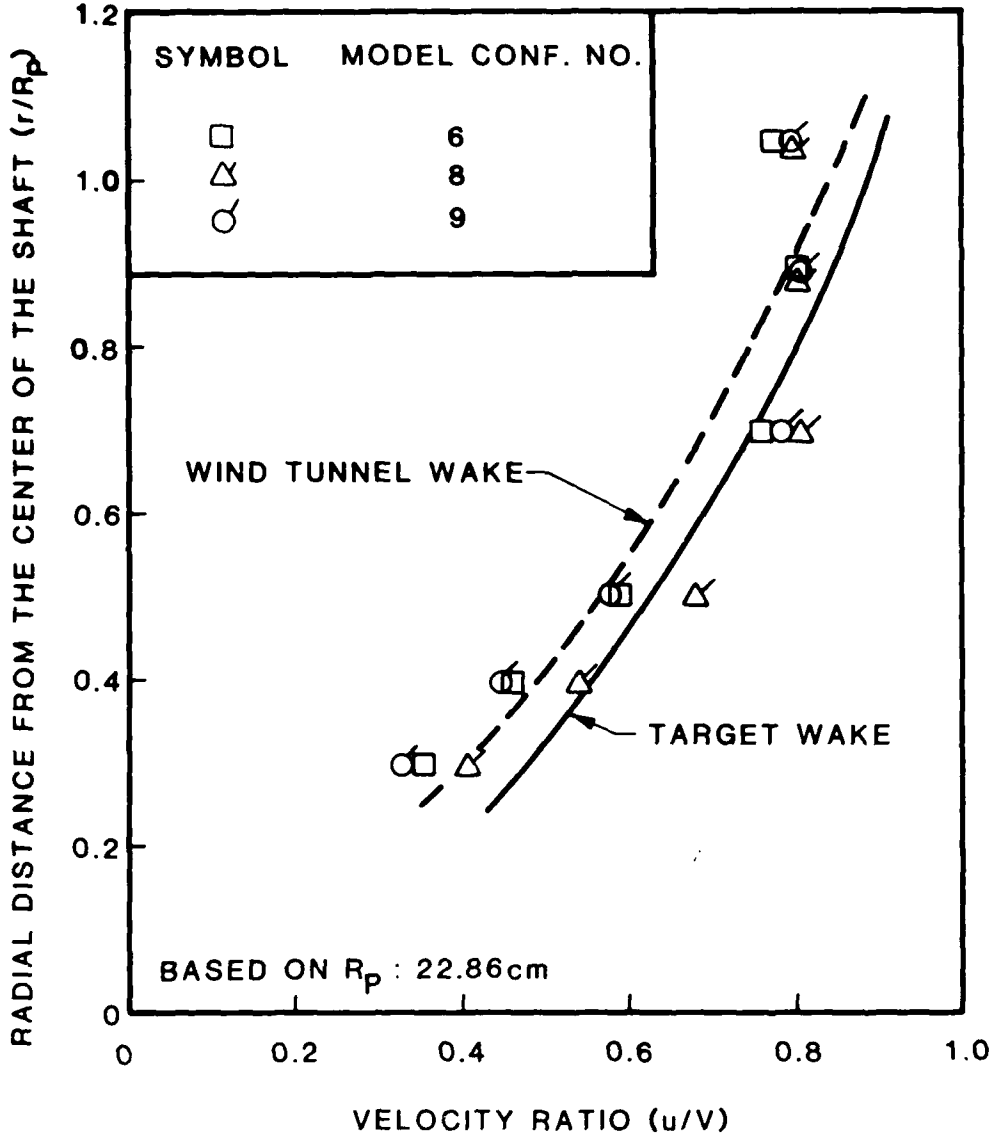

Figure 14 - Measured Velocity Distributions of Model Configurations 6,8 and 9

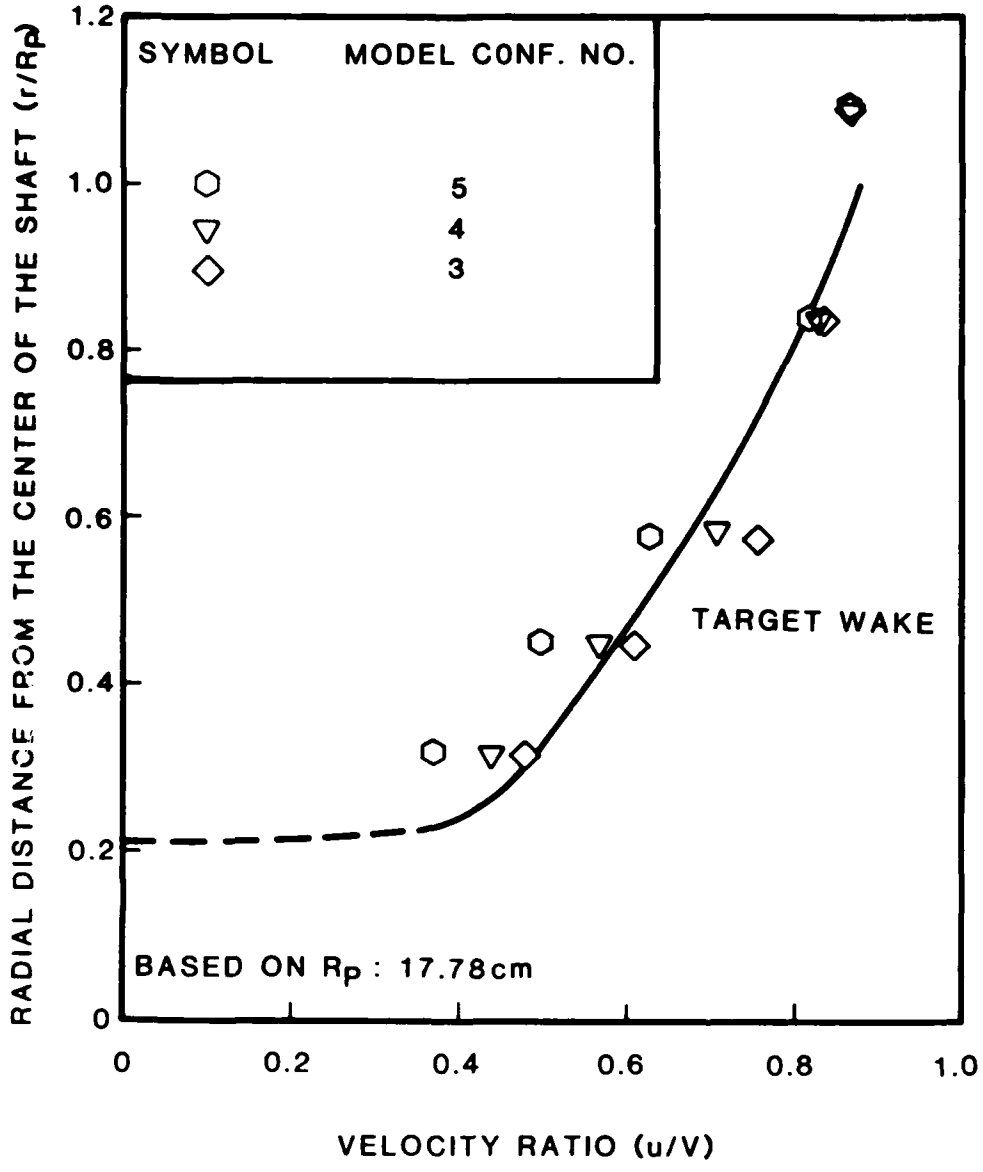

Figure 15 - Extrapolated Velocity Distributions of Model Configurations 3,4 and 5

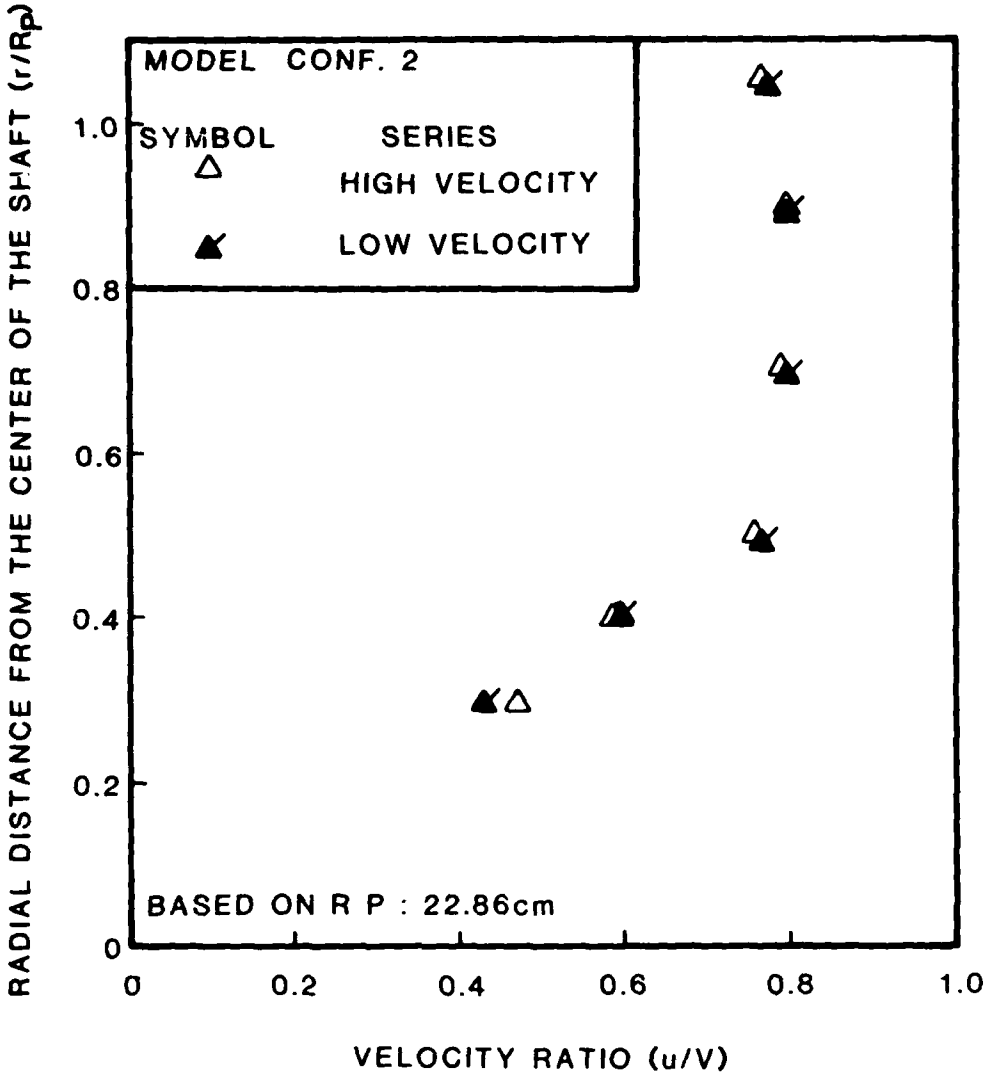

Figure 15a - A Comparison of Measured Velocity Distributions Between High and Low Velocity Series of Model Configuration 2

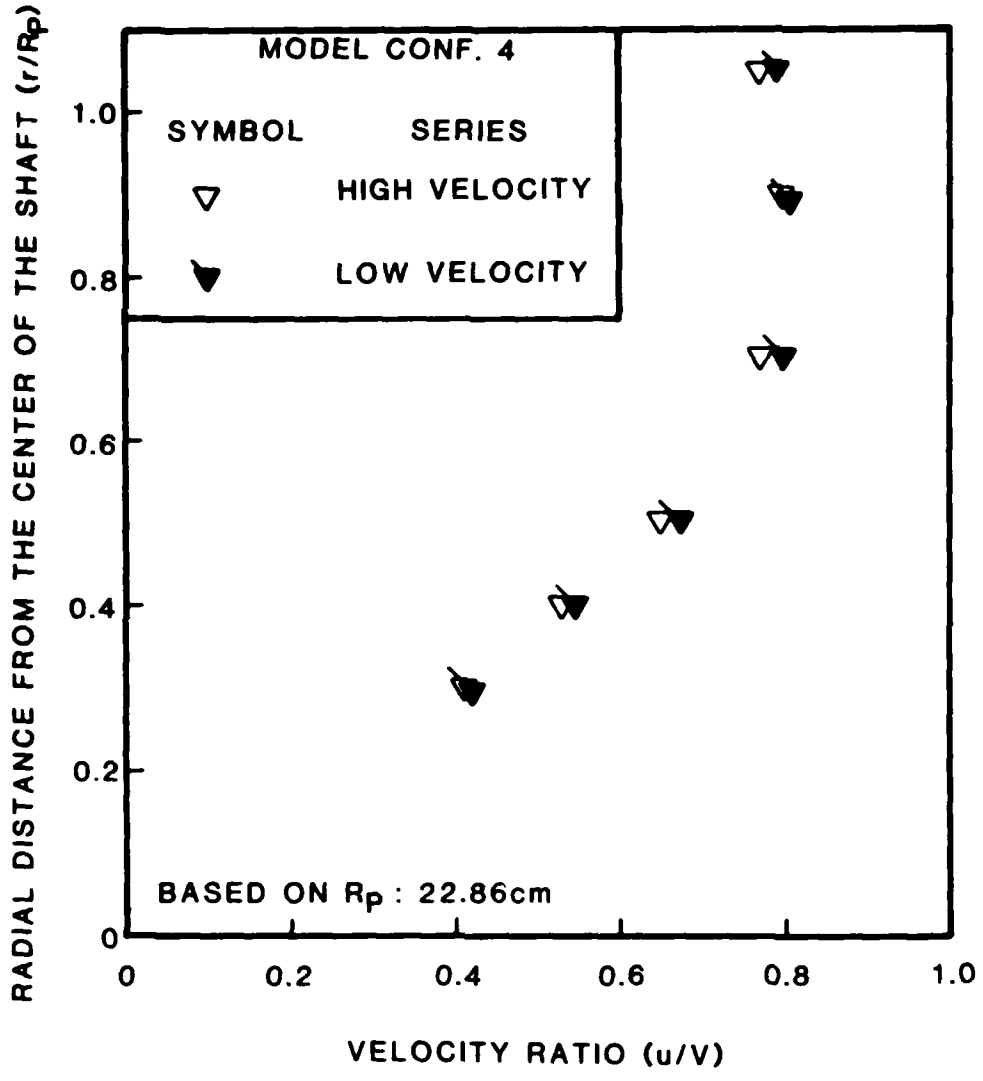

Figure 16b - A Comparison of Measured Velocity Distributions Between High and Low Velocity Series of Model Configuration 4

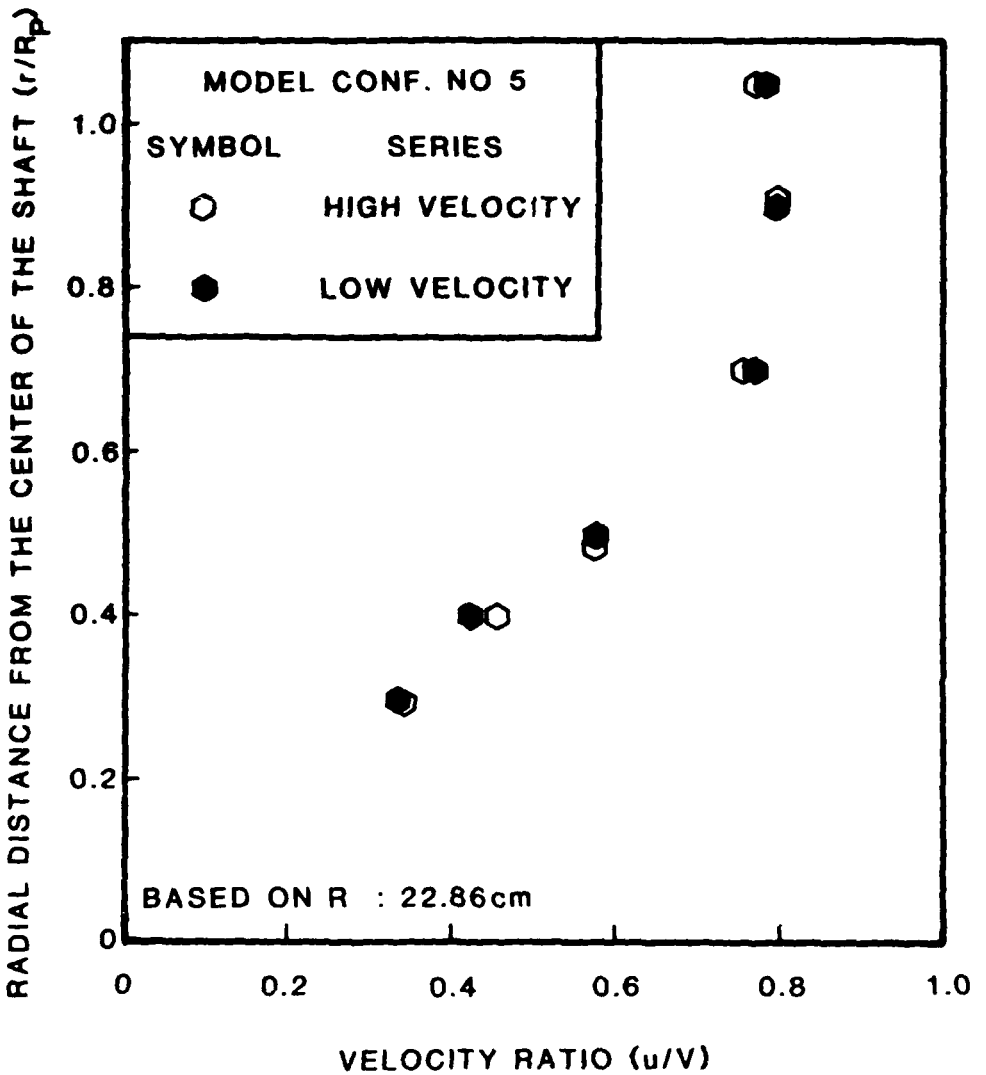

Figure 16c - A Comparison of Measured Velocity Distributions Between High and Low Velocity Series of Model Configuration 5

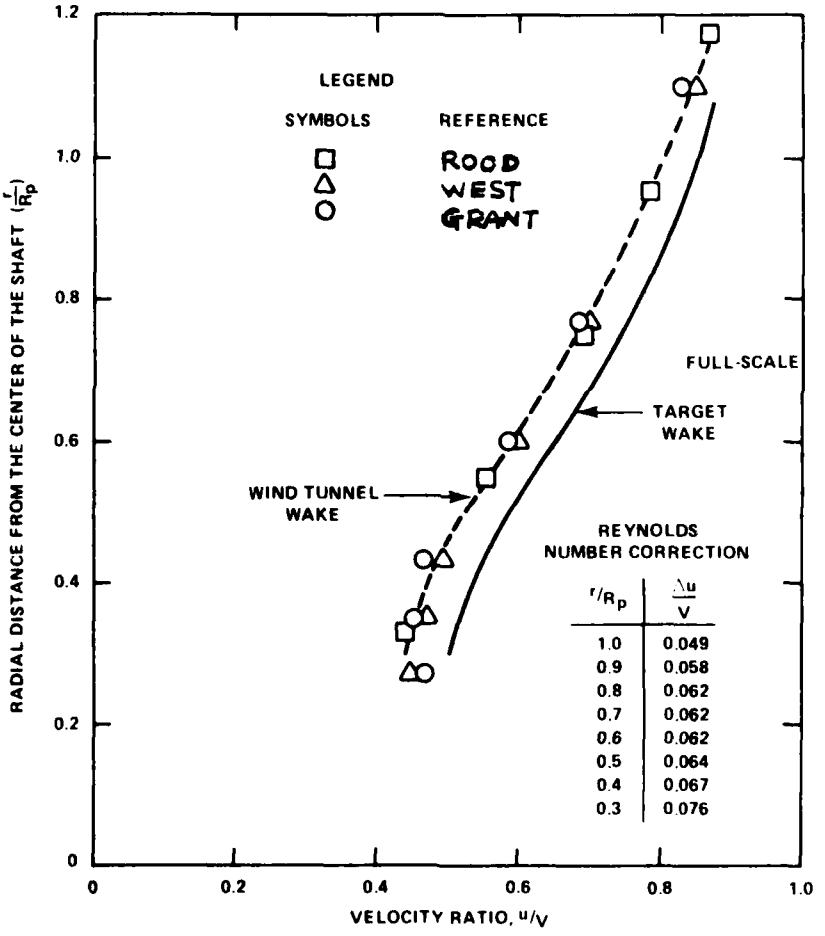

Figure 17- A Comparison Between Computed Full-Scale Target Wake and Measured Wind Tunnel Wake with Appendages

FIGURE 18 - THE SEMI-GEOSIM SHIP MODEL WITH APPENDAGES

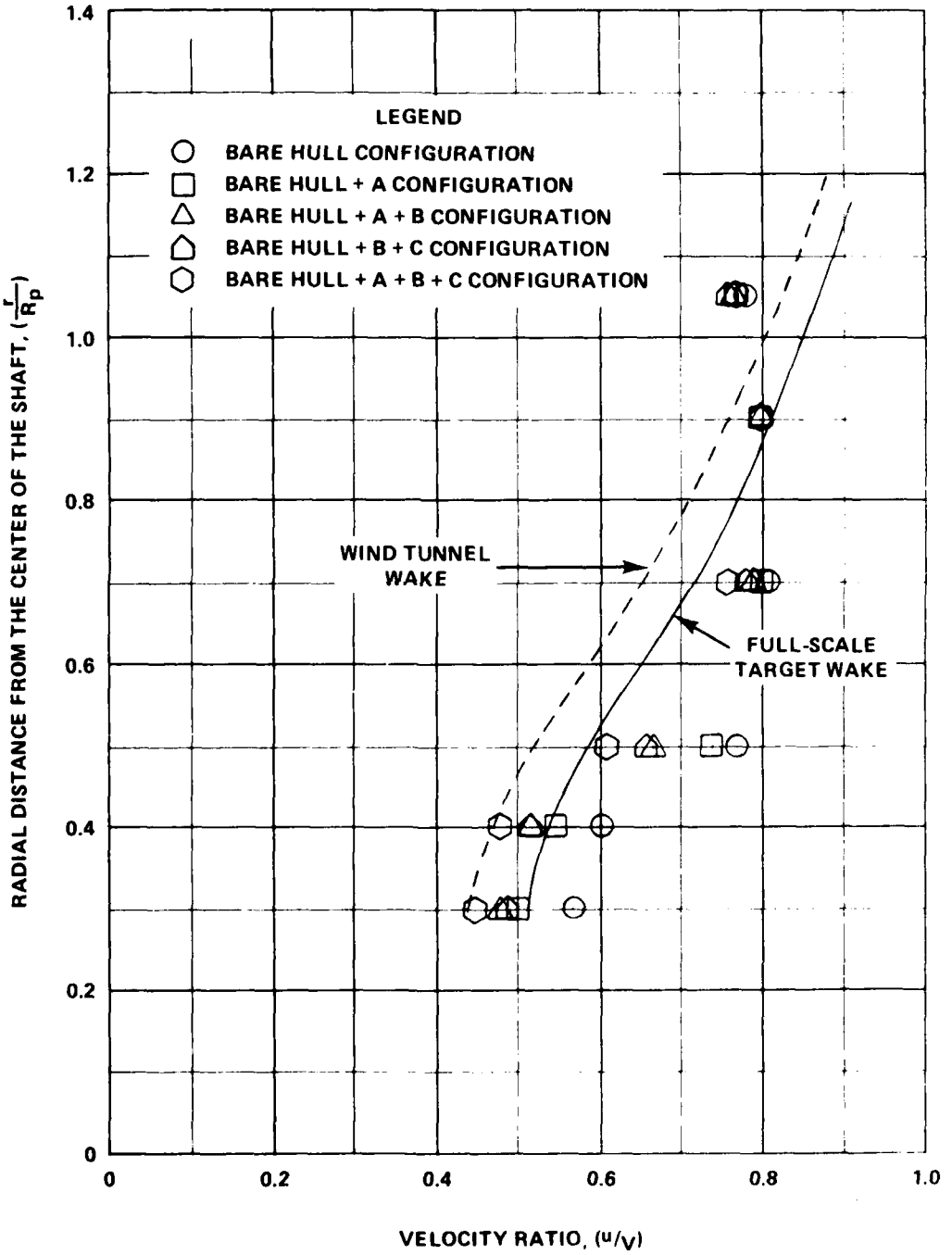

Figure 19 Measured Wake Data for D_p = 45.7 cm

PRECEDING PAGE BLANK-NOT FILMED

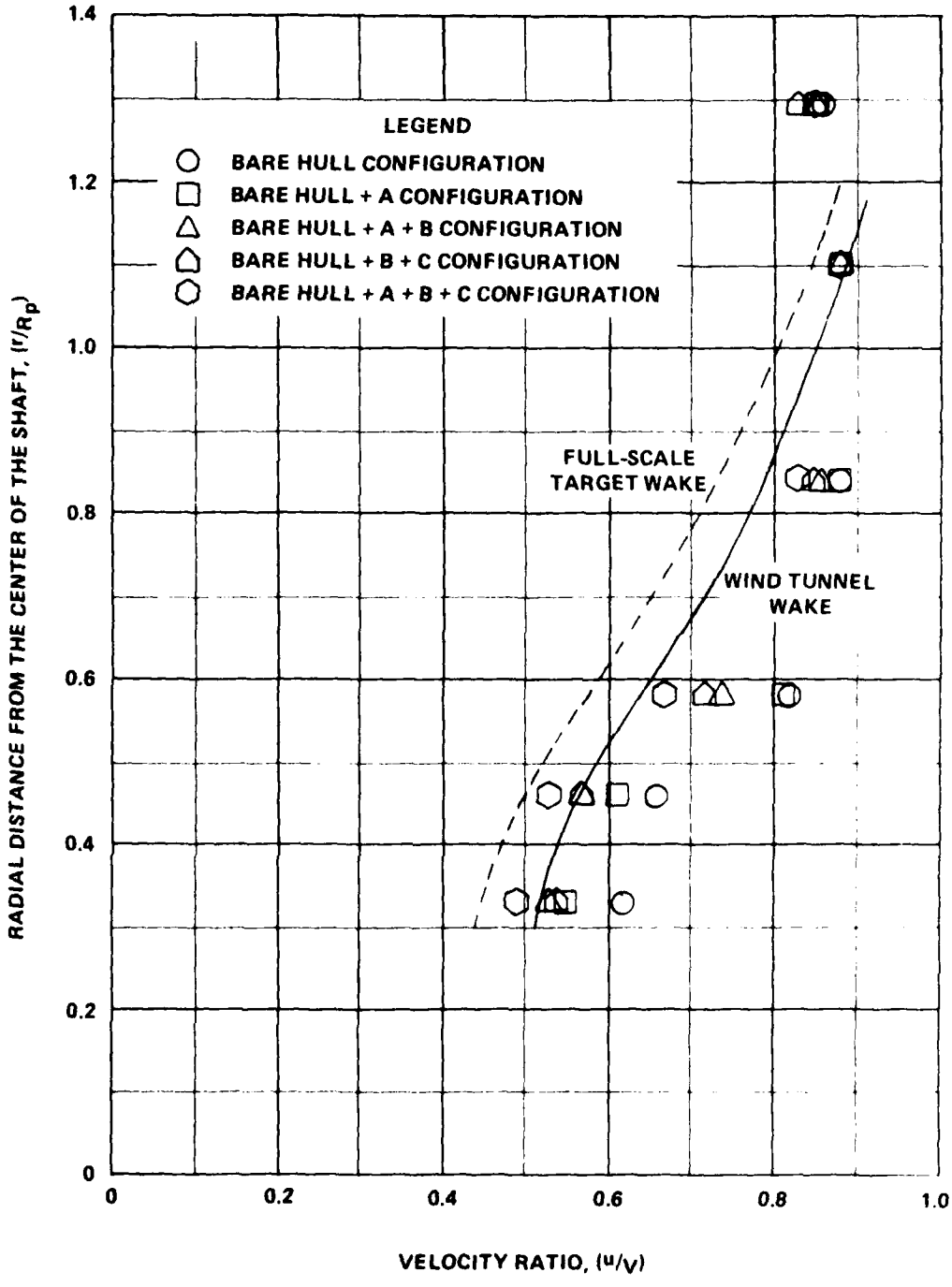

Figure 20 - Extrapolated Wake Data for D_p = 35.6 cm

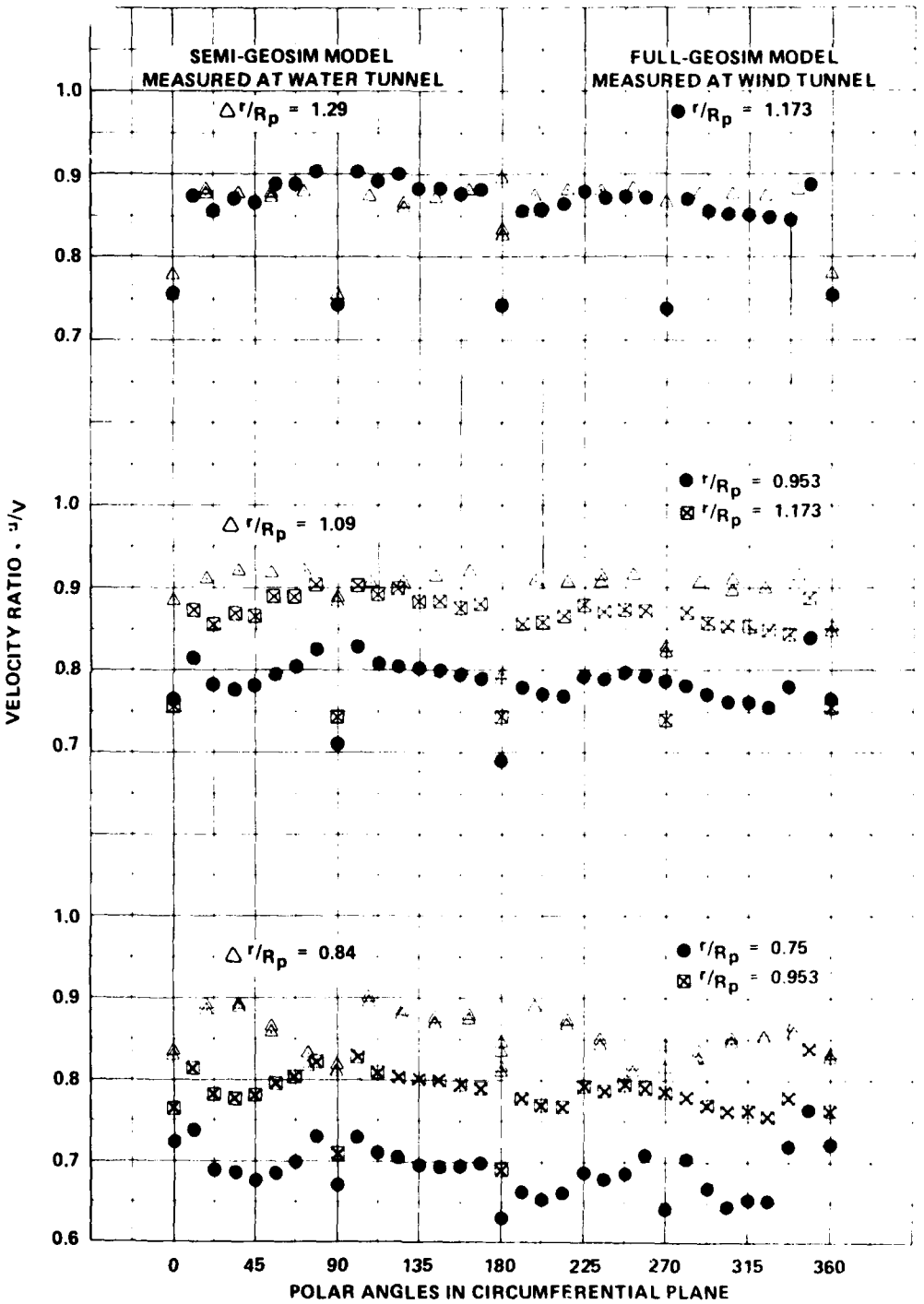

Figure 21a - Measured Local Velocity Distributions Along the Circumferential Planes for Model Configuration 5 at $\bar{r}/R_p$ = 1.29, 1.09, and 0.84 (D_p = 35.6 cm)

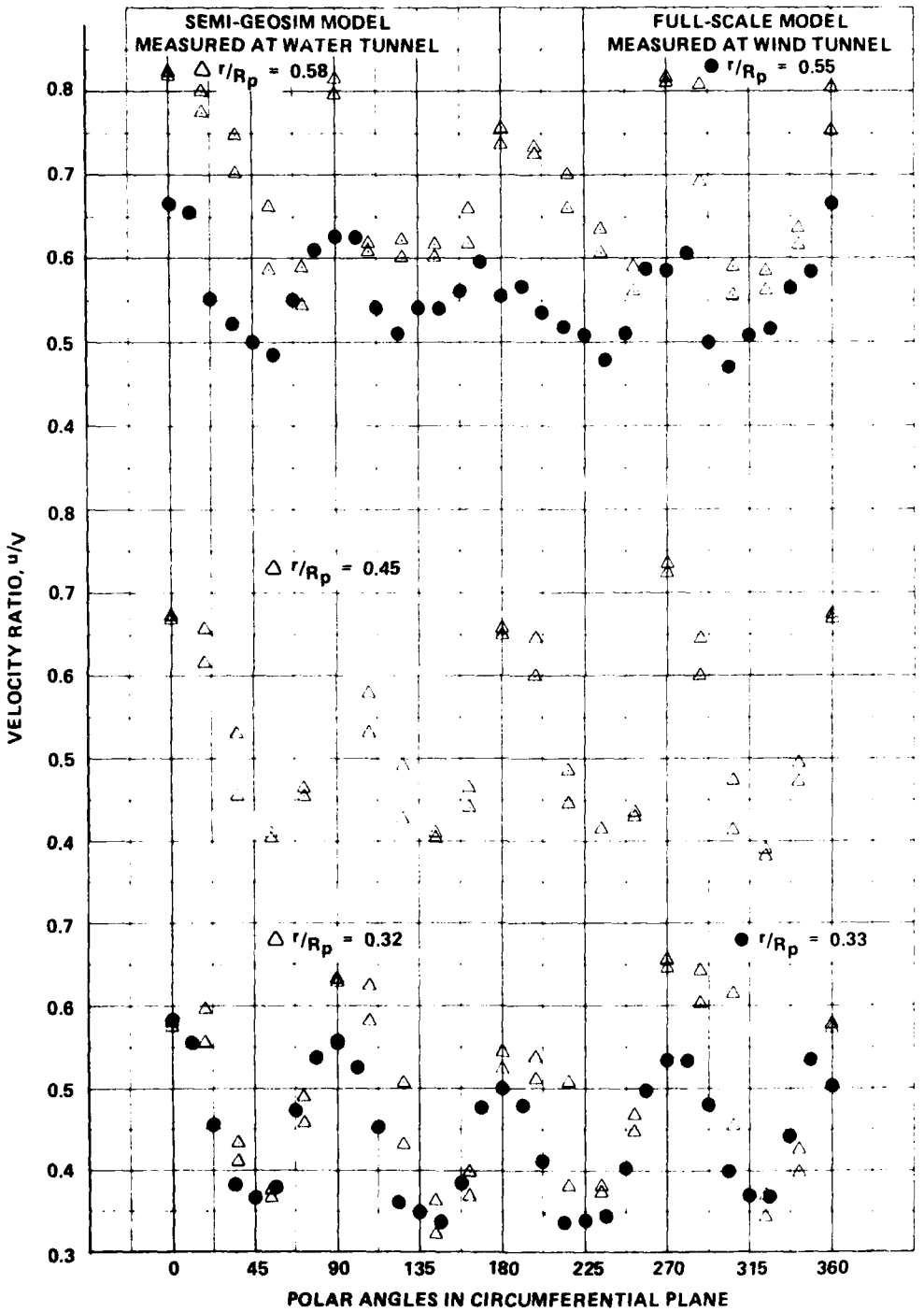

Figure 21b - Measured Local Velocity Distributions Along the Circumferential Planes for Model Configuration 5 at $\bar{r}/R_p$ = 0.58, 0.45, and 0.32 (D_p = 35.6 cm)

TABLE 1 - OFFSETS OF A REPRESENTATIVE SHIP WITH APPENDAGES REMOVED (Reference 5)

X/L	Y/L	X/L	Y/L	X/L	Y/L
0.0000	0.0000	0.2684	0.0456	0.7363	0.0427
0.0050	0.0100	0.2783	0.0456	0.7477	0.0421
0.0099	0.0142	0.2883	0.0456	0.7553	0.0416
0.0149	0.0175	0.2982	0.0456	0.7666	0.0408
0.0199	0.0202	0.3082	0.0456	0.7780	0.0399
0.0249	0.0227	0.3181	0.0456	0.7856	0.0392
0.0298	0.0248	0.3280	0.0456	0.7970	0.0382
0.0348	0.0268	0.3380	0.0456	0.8045	0.0375
0.0398	0.0287	0.3479	0.0456	0.8159	0.0363
0.0447	0.0303	0.3579	0.0456	0.8273	0.0350
0.0497	0.0319	0.3678	0.0456	0.8349	0.0341
0.0547	0.0333	0.3777	0.0456	0.8462	0.0326
0.0596	0.0347	0.3877	0.0456	0.8576	0.0310
0.0645	0.0359	0.3976	0.0456	0.8652	0.0299
0.0696	0.0370	0.4076	0.0456	0.8765	0.0281
0.0746	0.0381	0.4175	0.0456	0.8841	0.0268
0.0795	0.0390	0.4274	0.0456	0.8955	0.0248
0.0845	0.0399	0.4374	0.0456	0.9069	0.0226
0.0895	0.0407	0.4473	0.0456	0.9144	0.0211
0.0944	0.0414	0.4573	0.0456	0.9245	0.0189
0.0994	0.0421	0.4672	0.0456	0.9344	0.0166
0.1044	0.0427	0.4771	0.0456	0.9443	0.0140
0.1093	0.0432	0.4871	0.0456	0.9513	0.0122
0.1143	0.0437	0.4970	0.0456	0.9563	0.0108
0.1193	0.0441	0.5070	0.0456	0.9612	0.0095
0.1243	0.0444	0.5169	0.0456	0.9642	0.0087
0.1292	0.0447	0.5268	0.0456	0.9662	0.0081
0.1342	0.0450	0.5368	0.0456	0.9682	0.0076
0.1392	0.0452	0.5467	0.0456	0.9692	0.0074
0.1441	0.0453	0.5567	0.0456	0.9702	0.0072
0.1491	0.0454	0.5666	0.0456	0.9722	0.0068
0.1541	0.0455	0.5765	0.0456	0.9732	0.0066
0.1590	0.0448	0.5865	0.0456	0.9751	0.0063
0.1640	0.0456	0.5964	0.0456	0.9771	0.0062
0.1690	0.0456	0.6064	0.0456	0.9791	0.0059
0.1740	0.0456	0.6188	0.0456	0.9811	0.0056
0.1789	0.0456	0.6264	0.0455	0.9831	0.0053
0.1839	0.0456	0.6378	0.0455	0.9851	0.0050
0.1889	0.0456	0.6454	0.0455	0.9871	0.0048
0.1938	0.0456	0.6567	0.0453	0.9881	0.0046
0.1988	0.0456	0.6681	0.0452	0.9901	0.0043
0.2087	0.0456	0.6757	0.0450	0.9920	0.0040
0.2187	0.0456	0.6871	0.0448	0.9940	0.0036
0.2286	0.0456	0.6984	0.0444	0.9960	0.0028
0.2386	0.0456	0.7060	0.0441	0.9980	0.0019
0.2485	0.0456	0.7174	0.0437	1.0000	0.0000
0.2584	0.0456	0.7250	0.0433		

TABLE 2 - VELOCITY INCREMENTS DUE TO R_n CORRECTION

r/R_p	$\Delta u/V$
1.0	0.049
0.9	0.058
0.8	0.062
0.7	0.062
0.6	0.062
0.5	0.064
0.4	0.067
0.3	0.076

TABLE 3 - SUMMARY OF NINE MODEL CONFIGURATIONS

	1	2	3	4	5	6	7	8	9
PMB*	0	0.46	0.46	0.46	0.46	0.46	0.46	0.92	0.92
Type I**									
A	No	No	Yes	Yes	Yes	Yes	Yes	No	No
B	No	No	No	Yes	Yes	Yes	Yes	No	No
C	No	No	No	No	Yes	Yes	No	No	No
Type II***									
A	No	No	No	No	No	No	Yes	Yes	Yes
B	No	No	No	No	No	No	Yes	Yes	Yes
C	No	No	No	No	No	No	No	Yes	Yes
D	No	No	No	No	No	No	No	No	Yes
Shaft	No	No	Yes	Yes	Yes	No	No	No	No

*Parallel middle body measured in meters.

**Surface screen Type I.

***Surface screen Type II.

Surface screen on shaft housing.

TABLE 4 - MEASURED VELOCITY DISTRIBUTIONS IN METERS PER SECOND CORRESPONDING TO A 45.7 CENTIMETER PROPELLER

Pitot Tube	r cm	r/R_P	Model Configuration								
			1	2	3	4	5	6	7	8	9
6	24.00	1.05	10.58	10.52	10.46	10.58	10.70	10.73	10.36	6.68	6.71
5	20.57	0.9	11.09	10.94	10.88	10.97	11.09	11.06	10.79	6.71	6.80
4	16.00	0.7	10.88	10.85	10.55	10.61	10.51	10.52	10.58	6.71	6.61
3	11.43	0.5	10.76	10.39	9.51	8.96	8.01	8.20	8.63	5.67	4.91
2	9.14	0.4	9.08	8.23	7.68	7.19	6.37	6.37	6.98	4.51	3.81
1	6.86	0.3	6.58	6.04	6.00	5.61	4.76	4.88	5.33	3.41	2.83

TABLE 5 - VELOCITY RATIOS CORRESPONDING TO A 45.7 CENTIMETER PROPELLER

Pitot Tube	r cm	r/R_P	Model Configuration								
			1	2	3	4	5	6	7	8	9
6	24.00	1.05	0.76	0.77	0.77	0.77	0.77	0.77	0.78	0.79	0.79
5	20.57	0.9	0.80	0.80	0.80	0.80	0.80	0.80	0.80	0.80	0.80
4	16.00	0.7	0.79	0.79	0.78	0.77	0.76	0.76	0.78	0.80	0.78
3	11.43	0.5	0.78	0.76	0.70	0.65	0.58	0.59	0.64	0.68	0.58
2	9.14	0.4	0.66	0.60	0.56	0.53	0.46	0.46	0.52	0.54	0.45
1	6.86	0.3	0.47	0.44	0.44	0.41	0.34	0.35	0.40	0.40	0.33

TABLE 6 - EXTRAPOLATED VELOCITY DISTRIBUTIONS IN METERS PER SECOND CORRESPONDING TO A 35.6 CENTIMETER PROPELLER

Pitot Tube	r cm	$\bar{r}$ cm	$\bar{r}/R_P$	Model Configuration								
				1	2	3	4	5	6	7	8	9
6	24.00	22.94	1.29	10.58	10.52	10.46	10.58	10.70	10.73	10.36	6.68	6.71
5	20.57	19.51	1.10	11.09	10.94	10.88	10.97	11.09	11.06	10.79	6.71	6.80
4	16.00	14.94	0.84	10.88	10.85	10.55	10.61	10.51	10.52	10.58	6.71	6.61
3	11.43	10.36	0.58	10.76	10.39	9.51	8.96	8.01	8.20	8.63	5.67	4.91
2	9.14	8.08	0.45	9.08	8.23	7.68	7.19	6.37	6.37	6.98	4.51	3.81
1	6.86	5.78	0.32	6.58	6.04	6.00	5.61	4.76	4.88	5.33	3.41	2.83

TABLE 7 - VELOCITY RATIOS CORRESPONDING TO A 35.6 CENTIMETER PROPELLER

r cm	$\bar{r}$ cm	$\bar{r}/R_P$	Model Configuration					
			1	2	3	4	5	6
24.00	22.94	1.29	0.83	0.84	0.84	0.84	0.84	0.84
20.57	19.51	1.10	0.87	0.87	0.87	0.87	0.87	0.87
16.00	14.94	0.84	0.86	0.86	0.84	0.84	0.82	0.83
11.43	10.36	0.58	0.84	0.83	0.76	0.71	0.63	0.64
9.14	8.08	0.45	0.71	0.65	0.61	0.57	0.50	0.50
6.86	5.78	0.32	0.52	0.48	0.48	0.44	0.37	0.38

TABLE 8 - MEASURED VELOCITY DISTRIBUTIONS IN METERS PER SECOND IN LOW-VELOCITY SERIES

Pitot Tube	r cm	Model Configuration		
		2	4	5
6	24.00	5.06	5.15	5.24
5	20.57	5.18	5.21	5.36
4	16.00	5.18	5.21	5.15
3	11.43	4.91	4.39	3.90
2	9.14	3.84	3.44	2.80
1	6.86	2.77	2.65	2.26

TABLE 9 - VELOCITY RATIOS IN LOW-VELOCITY SERIES CORRESPONDING TO A 45.7 CENTIMETER PROPELLER

Pitot Tube	r/R_p	Model Configuration		
		2	4	5
6	1.05	0.78	0.79	0.78
5	0.9	0.80	0.80	0.80
4	0.7	0.80	0.80	0.77
3	0.5	0.76	0.67	0.58
2	0.4	0.59	0.53	0.42
1	0.3	0.43	0.41	0.34

Table 10 Measured Wake Data For D_p = 45.7 cm

PITOT TUBE NUMBER	$\frac{r}{R_p}$	MODEL CONFIGURATION				
		I	II	III	IV	V
6	1.05	10.1 m/s	10.0 m/s	10.0 m/s	10.0 m/s	10.2 m/s
5	0.9	10.3	10.3	10.4	10.6	10.6
4	0.7	10.4	10.3	10.2	10.3	10.0
3	0.5	9.6	9.5	8.7	8.7	8.1
2	0.4	7.7	7.1	6.7	6.9	6.4
1	0.3	7.3	6.4	6.2	6.5	5.9

Table 11 Nondimensional Measured Wake Data For D_p = 45.7 cm

PITOT TUBE NUMBER	$\frac{r}{R_p}$	MODEL CONFIGURATION u/V				
		I	II	III	IV	V
6	1.05	0.78	0.77	0.77	0.76	0.77
5	0.9	0.80	0.80	0.80	0.80	0.80
4	0.7	0.81	0.80	0.79	0.78	0.76
3	0.5	0.77	0.74	0.67	0.66	0.61
2	0.4	0.60	0.55	0.52	0.52	0.48
1	0.3	0.57	0.50	0.48	0.49	0.45

MODEL CONFIGURATION KEY

I – BARE HULL
II – BARE HULL WITH SCREEN A
III – BARE HULL WITH SCREEN A + B
IV – BARE HULL WITH SCREEN B + C
V – BARE HULL WITH SCREEN A + B + C

Table 12- Extrapolated Wake Data For D_p = 35.6 cm

PITOT TUBE NUMBER	$\frac{\bar{r}}{R_p}$	MODEL CONFIGURATION				
		I	II	III	IV	V
6	1.29	10.1 m/s	10.0 m/s	10.0 m/s	10.0 m/s	10.2 m/s
5	1.10	10.3	10.3	10.4	10.6	10.6
4	0.84	10.4	10.3	10.2	10.3	10.0
3	0.58	9.6	9.5	8.7	8.7	8.1
2	0.46	7.7	7.1	6.7	6.9	6.4
1	0.33	7.3	6.4	6.2	6.5	5.9

Table 13 Nondimensional Extrapolated Wake Data For D_p = 35.6 cm

PITOT TUBE NUMBER	$\frac{\bar{r}}{R_p}$	MODEL CONFIGURATION u/V				
		I	II	III	IV	V
6	1.29	0.86	0.85	0.85	0.83	0.85
5	1.10	0.88	0.88	0.88	0.88	0.88
4	0.84	0.88	0.88	0.86	0.85	0.83
3	0.58	0.82	0.81	0.74	0.72	0.67
2	0.46	0.66	0.61	0.57	0.57	0.53
1	0.33	0.62	0.55	0.53	0.54	0.49

MODEL CONFIGURATION KEY

I – BARE HULL
II – BARE HULL WITH SCREEN A
III – BARE HULL WITH SCREEN A + B
IV – BARE HULL WITH SCREEN B + C
V – BARE HULL WITH SCREEN A + B + C

REFERENCES

1. Ross, D., "Mechanics of Underwater Noise," Pargamon Press, Inc., New York (1976).

2. Strasberg, M., "Propeller Cavitation Noise after 35 Years of Study," Proceedings of Symposium on Noise and Fluid Engineering, American Society of Mechanical Engineers Annual Meeting, pp. 89-100 (1977).

3. Schlichting, H., "Boundary Layer Theory," McGraw-Hill Book Company, Inc., New York (1962).

4. Goodman, T.R., "Momentum Theory of a Propeller in a Shear Flow," Journal of Ship Research, Vol. 23, pp. 242-252 (Dec 1979).

5. Huang, T.T. et al., "Stern Boundary-Layer Flow on Axisymmetric Bodies," Twelfth Office of Naval Research Symposium on Naval Hydrodynamics, Washington, D.C. (Jun 1978).

6. Wang, H.T. and T.T. Huang, "Calculation of Potential Flow/Boundary Layer Interaction on Axisymmetric Bodies in Turbulent Boundary Layers," pp. 47-57, American Society of Mechanical Engineers, New York (Jun 1979).

7. Huang, T.T. and F.B. Peterson, "Influence of Viscous Effects on Model/Full-Scale Cavitation Scaling," Journal of Ship Research, Vol. 20, pp. 215-223 (Dec 1976).

8. Cox, B.D. and A.G. Hansen, "A Method for Predicting Thrust Deduction Using Propeller Lifting Surface Theory," DTNSRDC Report 77-0087 (Nov 1977).

9. Klebanoff, P.S. and Z.W. Diehl, "Some Features of Artificially Thickened Fully Developed Turbulent Boundary Layers with Zero Pressure Gradient," National Advisory Committee for Aeronautics Report 1110 (1952).

10. Robbins, B.E., "Experimental Axisymmetric Boundary-Layer Profile Modifications by the Addition of Surface Roughness Screens," Applied Research Laboratory Technical Memorandum TM 78-64 (Mar 1978).

11. Cebeci, T. and A.M.O. Smith, "Analysis of Turbulent Boundary Layers," Academic Press, New York (1974).

12. Bai, K.J., "Blockage Correction with a Free Surface," Journal of Fluid Mechanics, Vol. 94, pp. 433-452 (Nov 1979).

DTNSRDC ISSUES THREE TYPES OF REPORTS

1. DTNSRDC REPORTS, A FORMAL SERIES, CONTAIN INFORMATION OF PERMANENT TECHNICAL VALUE. THEY CARRY A CONSECUTIVE NUMERICAL IDENTIFICATION REGARDLESS OF THEIR CLASSIFICATION OR THE ORIGINATING DEPARTMENT.

2. DEPARTMENTAL REPORTS, A SEMIFORMAL SERIES, CONTAIN INFORMATION OF A PRELIMINARY, TEMPORARY, OR PROPRIETARY NATURE OR OF LIMITED INTEREST OR SIGNIFICANCE. THEY CARRY A DEPARTMENTAL ALPHANUMERICAL IDENTIFICATION.

3. TECHNICAL MEMORANDA, AN INFORMAL SERIES, CONTAIN TECHNICAL DOCUMENTATION OF LIMITED USE AND INTEREST. THEY ARE PRIMARILY WORKING PAPERS INTENDED FOR INTERNAL USE. THEY CARRY AN IDENTIFYING NUMBER WHICH INDICATES THEIR TYPE AND THE NUMERICAL CODE OF THE ORIGINATING DEPARTMENT. ANY DISTRIBUTION OUTSIDE DTNSRDC MUST BE APPROVED BY THE HEAD OF THE ORIGINATING DEPARTMENT ON A CASE-BY-CASE BASIS.